Institutionen för systemteknik
Department of Electrical Engineering

Examensarbete

Driveline Observer for an Automated Manual Gearbox

Examensarbete utfört i Fordonssystem
vid Tekniska högskolan i Linköping
av

Peter Juhlin-Dannfelt & Johan Stridkvist

LITH-ISY-EX--06/3828--SE

Linköping 2006

Linköpings universitet
TEKNISKA HÖGSKOLAN

Department of Electrical Engineering
Linköpings universitet
SE-581 83 Linköping, Sweden

Linköpings tekniska högskola
Linköpings universitet
581 83 Linköping

Driveline Observer for an Automated Manual Gearbox

Examensarbete utfört i Fordonssystem
vid Tekniska högskolan i Linköping
av

Peter Juhlin-Dannfelt & Johan Stridkvist

LITH-ISY-EX--06/3828--SE

Handledare: **Anders Fröberg**
ISY, Linköpings universitet
Fredrik Swartling
Scania CV AB
Mikael Hanson
Scania CV AB

Examinator: **Professor Lars Nielsen**
ISY, Linköpings universitet

Linköping, 21 June, 2006

Avdelning, Institution
Division, Department

Division of Vehicular Systems
Department of Electrical Engineering
Linköpings universitet
SE-581 83 Linköping, Sweden

Datum
Date

2006-06-21

Språk
Language

☐ Svenska/Swedish
☒ Engelska/English
☐ ____________

Rapporttyp
Report category

☐ Licentiatavhandling
☒ Examensarbete
☐ C-uppsats
☐ D-uppsats
☐ Övrig rapport
☐ ____________

URL för elektronisk version
`http://www.fs.isy.liu.se`
`http://www.ep.liu.se`

ISBN
—

ISRN
LITH-ISY-EX--06/3828--SE

Serietitel och serienummer
Title of series, numbering

ISSN
—

Titel
Title

Drivlineobservatör för en Automatiserad Manuell Växellåda
Driveline Observer for an Automated Manual Gearbox

Författare
Author

Peter Juhlin-Dannfelt & Johan Stridkvist

Sammanfattning
Abstract

The Automated Manual Transmission system Opticruise is dependent on signals from sensors located in different parts of the Scania trucks. These signals are of different qualities and have different update frequencies. Some signals and quantities that are hard or impossible to measure are also of importance to this system.

In this thesis a driveline observer for the purpose of signal improvement is developed and estimations of unknown quantities such as road incline and mass of the vehicle are performed. The outputs of the observer are produced at a rate of 100 Hz, and include in addition to the mass and road incline also the speed of the engine, output shaft of the gearbox, wheel and the torsion in the driveline. Further the use of an accelerometer and the advantages gained from using it in the observer are investigated.

The outputs show an increased quality and much of the measurement noise is successfully removed without introducing any time delays. A simulation frequency of 100 Hz is possible, but some dependency toward the stiffness of the driveline is found. The observer manages to estimate the road slope accurately. With the use of an accelerometer the road slope estimation is further improved and a quickly converging mass estimation is obtained.

Nyckelord
Keywords driveline, observer, road slope, mass, accelerometer

Abstract

The Automated Manual Transmission system Opticruise is dependent on signals from sensors located in different parts of the Scania trucks. These signals are of different qualities and have different update frequencies. Some signals and quantities that are hard or impossible to measure are also of importance to this system.

In this thesis a driveline observer for the purpose of signal improvement is developed and estimations of unknown quantities such as road incline and mass of the vehicle are performed. The outputs of the observer are produced at a rate of 100 Hz, and include in addition to the mass and road incline also the speed of the engine, output shaft of the gearbox, wheel and the torsion in the driveline. Further the use of an accelerometer and the advantages gained from using it in the observer are investigated.

The outputs show an increased quality and much of the measurement noise is successfully removed without introducing any time delays. A simulation frequency of 100 Hz is possible, but some dependency toward the stiffness of the driveline is found. The observer manages to estimate the road slope accurately. With the use of an accelerometer the road slope estimation is further improved and a quickly converging mass estimation is obtained.

Preface

This thesis completes our studies at Linköping University for a Master of Science in Applied Physics and Electrical Engineering. It has been an interesting and challenging work and we have gotten plenty of opportunities to put knowledge gained during our education to practice.

Writing this thesis at Scania has been extremely stimulating and trucks have become a more and more exciting application over time.

Outline

In the introductory chapter of the thesis the purpose and method of the thesis is presented. Model equations for the driveline model are presented in the second chapter. These equations form the basis for the observer and in chapter three and four the different signals and parameters used in the model are examined. In chapter five the model is simulated and validated against measurements.

Chapter six contains some basic theory for observers which is used together with the driveline model in chapter seven. The drive resistance which up to now has been considered an input is modeled in chapter eight and in chapter nine this model is included in the driveline model and an estimation of the road slope is made. The parameter sensitivity and the use of different measured signals is examined in chapter ten.

An accelerometer is examined in chapter 11 and with its use an estimation of the road slope is made. An adaptive mass estimation is also presented in this chapter. Finally, in chapter 12 and 13 a final validation of the observer is made, conclusions are drawn and some extensions for the thesis are presented.

Acknowledgment

We would like to express our greatest gratitude to our supervisors at Scania Fredrik Swartling and Mikael Hanson, who have always had time for our questions and helped us in any way possible. The group NET deserves a big thank for letting us feel as members of the staff and for answering a lot of questions about trucks that have come up during the course of this thesis. Anders Fröberg, who has given insightful comments and tips from time to time also has a part in this thesis.

Finally we would like to thank our girlfriends for providing shelter during our many visits to Linköping during this spring and for supporting us.

Johan Stridkvist and Peter Juhlin-Dannfelt, Södertälje, 2006

Contents

1 Introduction **1**
1.1 Objective 2
1.2 Method 2
1.3 Assumptions and Limitations 2

2 Model of the Driveline **3**
2.1 Engaged Driveline 3
2.1.1 State-Space Model for the Engaged Driveline 7
2.2 Disengaged Driveline 10
2.2.1 State-Space Model for the Disengaged Driveline 10
2.3 Switching Between Engaged and Disengaged Mode 11
2.4 Simulation Environment 13

3 Signals **15**
3.1 The Torques 15
3.2 Velocities 16
3.3 State of the Gearbox 17

4 Parameters **19**
4.1 The Driveline Parameters 19
4.2 Estimating Unknown Parameters 19
4.2.1 Estimation Using Integration of Angular Velocities 21
4.2.2 Estimation Based on Oscillations in the Driveline 22
4.2.3 Parameter Sensitivity of the Parameter Estimation 28
4.3 Sensitivity Analysis of the Driveline Model 29
4.3.1 Differentiating the Driveline Model 29
4.3.2 Simulating the Driveline 29
4.4 Results and Summary 36

5 Simulation and Validation of the Driveline Model **37**
5.1 Simulations Using Recordings from the Truck ”Mastodont” 37
5.2 Simulations Using Recordings from the Truck ”Melvin” 41

6 Basic Theory for the Observer **45**
6.1 Discretization . . . 45
6.2 Observer and Kalman Filtering . . . 46
6.3 Calculating the Covariance Matrices . . . 47
6.4 Motivating the Use of a Kalman Filter . . . 48
6.5 Extending the Model with Noise States . . . 49

7 Observer Design **51**
7.1 Observability of the Model . . . 51
7.2 Designing the Observer . . . 51
7.3 Implementation . . . 52
7.4 Evaluation . . . 52
7.5 Observer with Measurement Offset . . . 55
  7.5.1 Estimating the Rolling Radius . . . 57
7.6 Observer with Modeled Measurement Noise . . . 58
  7.6.1 Modeling the Noise . . . 59
7.7 Summary . . . 60

8 Modeling the Drive Resistance **63**
8.1 The Rolling Resistance . . . 63
8.2 The Air Resistance . . . 64
8.3 Road Incline . . . 64
8.4 The Drive Resistance Model . . . 64
8.5 Identification of the Drive Resistance Parameters . . . 65
8.6 Implementation of the Drive Resistance . . . 66
8.7 Summary . . . 66

9 Observer Design with Non-Linear Drive Resistance Model **67**
9.1 Linearizing the Drive Resistance . . . 67
9.2 Kalman Filter Design Methods for the Non-Linear System . . . 68
9.3 Choosing Linearization Points . . . 68
9.4 Estimating the Road Slope . . . 68
  9.4.1 Spike Reduction in the Road Slope Estimation . . . 69
  9.4.2 Comparison between Drive Resistance Parameters . . . 70
9.5 The Disc Brakes . . . 72
9.6 Summary . . . 72

10 Sensor and Parameter Analysis **73**
10.1 Sensor signals . . . 73
  10.1.1 Method . . . 73
  10.1.2 Comparison Between the Transmission Speed Sensors . . . 74
  10.1.3 Different Sensor Configurations . . . 75
  10.1.4 Conclusions . . . 75
10.2 Parameter Sensitivity . . . 76
  10.2.1 Method . . . 76
  10.2.2 Conclusions . . . 77

11 Contributions from an Accelerometer **79**
11.1 The Sensor 79
11.2 Calibration 80
11.3 Road Incline Estimation 80
11.4 Evaluation of the Road Slope Filter 81
11.5 Compensating for Perpendicular Acceleration 81
11.6 Combining the Accelerometer with the Observer 83
11.7 Estimation of Brake Torque 83
11.8 Mass Estimation 83
11.9 Summary 87

12 Simulation and Validation of the Observer **89**
12.1 Speed Signals and Torsion 89
12.2 Road Slope 92
12.3 Use of Disc Brakes during a Gear Shift 92

13 Conclusions and Future Work **95**
13.1 Conclusions 95
13.2 Future Work 96

Bibliography **103**

A Truck Information **105**
A.1 Mastodont 105
A.2 Melvin 107

B Simulink Models **108**

Chapter 1

Introduction

The department of Transmission Software (NET) at Scania in Södertälje is responsible for a number of systems which mainly concerns the transmission. Their main work fields lies in the retarder (for further information refer to chapter 3.1), all wheel drive and Opticruise software. This thesis has its focus on the aspects of the Opticruise system.

The Scania Opticruise system is an automated gear shift system that uses a manual gearbox. Opticruise replaces the gear lever with pneumatics and a control unit. A gear shift using Opticruise consists of five phases, as illustrated in figure 1.1. In phase one, the torque in the gearbox is controlled to zero in order to make it possible to disengage the dog clutches in the gearbox. The disengagement is performed during phase two, meaning that the gearbox is put into neutral gear. In phase three, the engine speed is controlled to match the speed of the output shaft of the gearbox for the new gear. This is a sensitive part of the gear shift since there is no connection between the engine and the wheels, which makes the synchronization time critical. The fourth phase consists of the engagement of the dog clutches. In phase five, torque is once again applied to the gearbox and the gear shift is completed. Opticruise and the other systems NET is responsible for

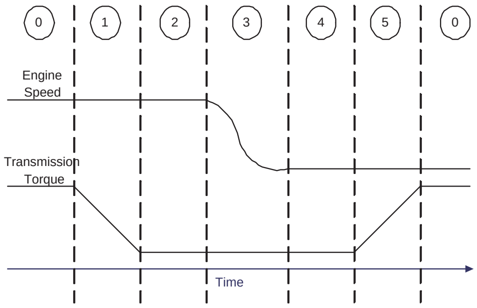

Figure 1.1. The different phases of a gear shift with Opticruise.

are dependent on signals from sensors in different parts of the truck. These signals are transmitted either directly to the Opticruise system or over the internal bus-network, called the CAN-bus. The different signals have different resolutions and update frequencies, and since the controller works at a rate of 100 Hz, the signals working at a lower update frequency are considered constant at times when no new information is available. This is of course not optimal for most applications, even though for some it might be enough.

Some information needed in the Opticruise system is not measured, and different methods are used to estimate this. Important non-measurable information is the mass of the vehicle and the drive resistance, which consists of rolling resistance, air resistance and force of gravity. This information is of importance in for example the gear selection process, and therefore possibilities to make better estimations are of great interest.

1.1 Objective

The goal of this thesis is to develop an observer for the driveline which at a frequency of 100 Hz produce the angular velocities of the engine, the output shaft of the gearbox and wheel with a reduced noise level. The observer shall contain a model for the drive resistance. Estimations of the road slope and mass shall be obtained from the observer. The advantages gained from using an accelerometer shall be investigated.

1.2 Method

A driveline model based on rotating inertias and damped shaft flexibilities is derived. The model is primarily developed from literature studies. Weaknesses of the model are iteratively found and solutions to the problems are proposed and evaluated. A stationary Kalman filter is designed for the model and is used as an observer. By testing the observer as often as possible, finding bugs becomes easier. By developing different modules for different parts of the observer, it is easier to evaluate different observers. The development of the observer is performed in Matlab and Simulink, and simulations are made off-line. An accelerometer is mounted on the truck and an investigation concerning mounting location is made. Methods for including the accelerometer signal in the driveline observer are tested.

1.3 Assumptions and Limitations

Assumptions given in this section are valid for the entire thesis, unless something else is stated. The inputs are assumed to be constant between updates. Slip is assumed not to be present, meaning that the speed of the vehicle v and the angular velocity of the wheel ω_w satisfy $v = r_w \omega_w$, where r_w is the rolling radius of the wheel. Time delays are not considered in this thesis. Only recordings from two trucks are available for this thesis.

Chapter 2

Model of the Driveline

A model of the driveline for an engaged and disengaged gearbox is developed. The driveline consists of the parts seen in figure 2.1, starting with the output from the engine. Numerous papers are written about models of the driveline for the purpose of control systems. The equations are usually the same and can for example be seen in [1], [2] and [3]. In this chapter these equations are stated and simplifications suitable for the applications in this thesis are made.

The models consist of rotating inertias connected by damped shaft flexibilities representing the different parts of the driveline. The complexity of the model is determined by the frequency of oscillation that is considered, which usually is the first mode of oscillation, see [4]. In the model developed here, no oscillations above the first mode are intended to be captured. Creating a model for both the engaged and disengaged gearbox makes the model more complex since it is divided into two models. In this chapter the different subsystems of the driveline are described. These can be seen together with their respective variables in figure 2.2. The generalized Newton's second law is used to derive the equations for the inertias. The different shafts and the clutch are seen as damped springs.

2.1 Engaged Driveline

Since the purpose of this work is to create an observer that works both when the gearbox is engaged and disengaged, two different models are developed. In this section a model of an engaged driveline is derived. Figure 2.2 shows the labels of the inputs and outputs of each subsystem.

Engine

The engine output torque is given by the driving torque from the combustion T_{comb}, the internal friction torque of the engine $T_{fr,e}$, the torque taken by external equipment such as air conditioner $T_{parasitic}$, the torque from the exhaust brake T_{exh} and the load from the clutch T_c. This yields for the rotational speed of the

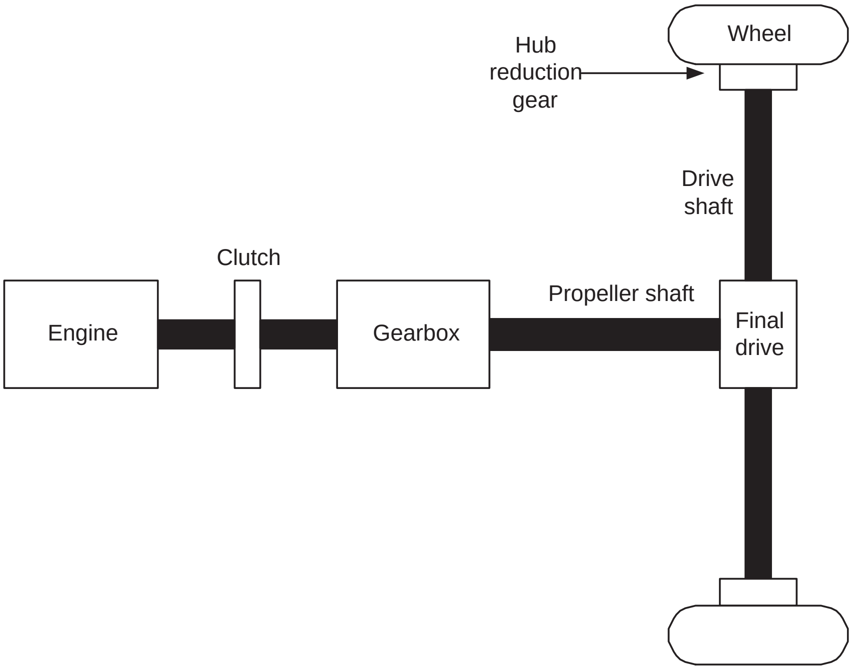
Wheel
Hub
reduction
gear
Drive
shaft
Clutch
Propeller shaft
Engine
Gearbox
Final
drive

Figure 2.1. The Driveline.

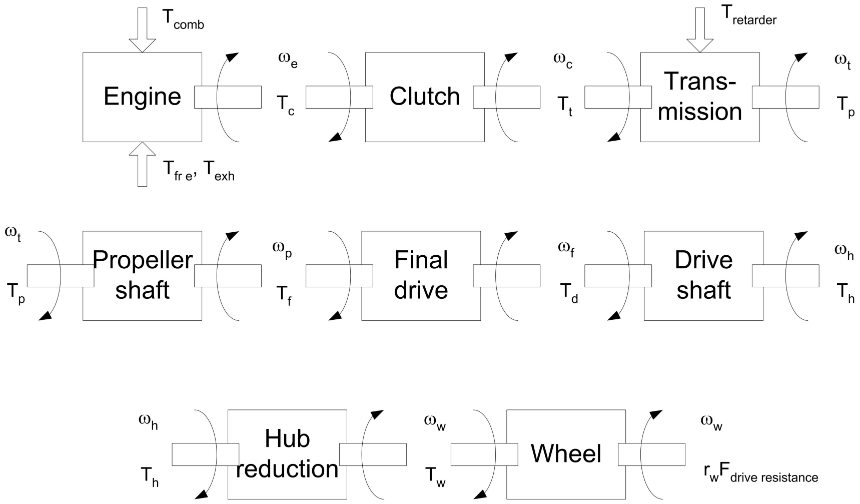
T_{comb}
$T_{retarder}$
Engine
ω_e
T_c
Clutch
ω_c
T_t
Trans-
mission
ω_t
T_p
$T_{fr\,e}$, T_{exh}
ω_t
T_p
Propeller
shaft
ω_p
T_f
Final
drive
ω_f
T_d
Drive
shaft
ω_h
T_h
ω_h
T_h
Hub
reduction
ω_w
T_w
Wheel
ω_w
$r_w F_{drive\ resistance}$

Figure 2.2. The subsystems of the driveline with labels to the respective variables.

engine flywheel ω_e with inertia J_e

$$J_e\dot{\omega}_e = T_{comb} - T_{fr,e} - T_{parasitic} - T_c - T_{exh} \tag{2.1}$$

Clutch

The clutch connects the engine flywheel to the input shaft of the gearbox. In this work, the clutch is assumed always to be engaged, which is the case in the Opticruise system except during take off. The clutch is seen as a damped spring where the transmitted torque depend on the angular difference $\theta_e - \theta_c$ and the difference in angular speed $\omega_e - \omega_c$. The speed of the output shaft of the clutch is denoted ω_c.

$$\begin{aligned} T_c &= T_t = k_c(\theta_e - \theta_c) + c_c(\omega_e - \omega_c) && (2.2)\\ \dot{\theta}_e &= \omega_e && (2.3)\\ \dot{\theta}_c &= \omega_c && (2.4) \end{aligned}$$

where k_c is the stiffness of the clutch, c_c is the damping coefficient of the clutch and T_t is the torque acting on the input shaft of the gearbox.

Gearbox

The gearbox consists of a number of rotating inertias which are coupled to give different gear ratios i_t. The gearbox is described by the equations

$$\begin{aligned} \theta_c &= \theta_t i_t \Rightarrow \omega_c = \omega_t i_t && (2.5)\\ J_t\dot{\omega}_t &= T_t i_t - T_p - b_t\omega_t - T_{retarder} && (2.6) \end{aligned}$$

where J_t is all the inertias of the gearbox lumped together on the outgoing shaft, which rotates with the speed ω_t. The load torque from the propeller shaft is T_p. The inertia varies depending on which gear that is currently engaged. The friction in the gearbox is assumed to be proportional to the angular velocity of the gearbox's output shaft with the proportional constant b_t. $T_{retarder}$ is the torque generated by the hydraulic retarder brake that acts on the output shaft of the gearbox. The speed of the output shaft of the gearbox is for the remainder of this thesis denoted transmission speed, ω_t.

Propeller Shaft

The propeller shaft connects the output shaft of the gearbox to the input shaft of the final drive, and is described in the same way as the clutch, i.e. as a damped flexible shaft:

$$T_p = T_f = k_p(\theta_t - \theta_p) + c_p(\omega_t - \omega_p) \tag{2.7}$$

Here, k_p is the stiffness and c_p is the damping of the propeller shaft while ω_p represents the speed of the propeller shaft at the input of the final drive. T_f is the torque acting on the input of the final drive.

Final Drive

The final drive is just like the gearbox a torque/velocity transformer. While the gearbox has several gear ratios, the final drive just has one, i_f.

$$\begin{aligned}\theta_p &= \theta_f i_f \Rightarrow \omega_p = \omega_f i_t && (2.8)\\ J_f \dot{\omega}_f &= T_f i_f - b_f \omega_f - T_d && (2.9)\end{aligned}$$

Here, ω_p is the speed of the input shaft, i.e. the propeller shaft and ω_f is the speed of the output shaft of the final drive. T_d is the load from the drive shaft.

Drive Shaft

The drive shaft connects the final drive to the hub reduction gear if the vehicle is equipped with one, otherwise it is connected to the wheel. It is described in the same way as the clutch and the propeller shaft:

$$T_h = T_d = k_d(\theta_f - \theta_h) + c_d(\omega_f - \omega_h) \tag{2.10}$$

Here, k_d is the stiffness and c_d is the damping of the drive shaft while ω_h represents the speed of the drive shaft at the hub reduction gear. T_h is the torque acting on the input of the hub reduction gear.

Hub Reduction Gear

In some situations it may be preferred to have a smaller torque acting on the drive shaft. If this is the case, the truck can be equipped with a hub reduction gear at the end of the drive shaft. This is a planetary gear working as a second final gear. If the truck is equipped with a hub reduction gear, the final gear usually has a transmission ratio of one or close to one. The hub reduction gear is described as a transmission without any inertia, making it a pure transformation of the torque and angular velocity with the gear ratio i_h:

$$\omega_h = \omega_w i_h, \quad T_h i_h = T_w \tag{2.11}$$

where ω_w is the wheel speed and T_w is the driving torque acting on the wheel.

Wheel

The forces acting on the truck with mass m and speed v give together with Newton's second law

$$F_w = m\dot{v} + F_{dr} \tag{2.12}$$

where F_w is the driving force and the driving resistance force F_{dr} includes rolling resistance, air drag and the resistance from the gravitational force. If no slip is assumed, $v = r_w \omega_w$, Newton's second law gives

$$(J_w + m r_w^2)\dot{\omega}_w = T_w - T_{dr} \tag{2.13}$$

for the wheel, where $T_{dr} = r_w F_{dr}$ and J_w is the moment of inertia of the wheels.

2.1.1 State-Space Model for the Engaged Driveline

The equations for the different parts of the driveline given in the previous section can be used to form a state-space model of the driveline. The complexity of the driveline does however become unnecessarily high. The moment of inertia of the final drive is much smaller than the other inertias, which makes the propeller shaft and drive shaft act as one flexibility, see [4].

The amount of dynamic between the engine and gearbox is also questionable. The engine speed and the transmission speed while driving on the highest gear can be seen in figure 2.3. Here just a small difference can be seen, and based upon this, a first approach is to neglect this difference between the velocities in the model. The difference between the two angular velocities does however make a difference just after a gear shift. In figure 2.4 it can be seen, that right after a gear shift there is a settling time before the two velocities have reached the same level. To try and take this into account, the synchronization between the engine and transmission speed is modeled. The synchronization can be seen as a friction between the cogwheels in the gearbox when they are put together. This problem will be discussed further in section 2.3.

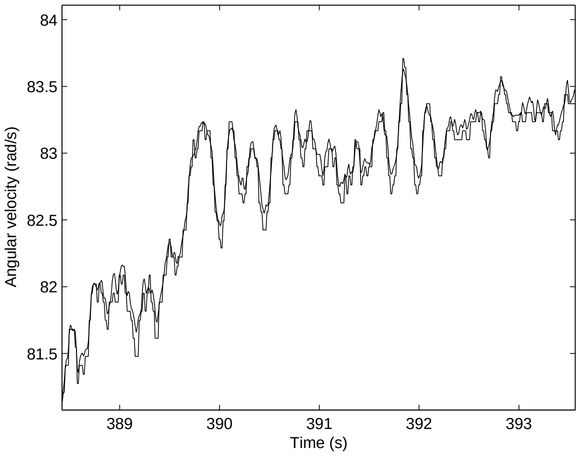

Figure 2.3. Engine (scaled) and transmission speed.

Model Reduction

The driveline model in equations (2.1)-(2.13) is reduced according to what is written previously in this section. The clutch and the propeller shaft are said to be stiff, which convert equations (2.4) and (2.7) to

$$T_c = T_t, \quad \theta_e = \theta_c \tag{2.14}$$

$$T_p = T_f, \quad \theta_t = \theta_p \tag{2.15}$$

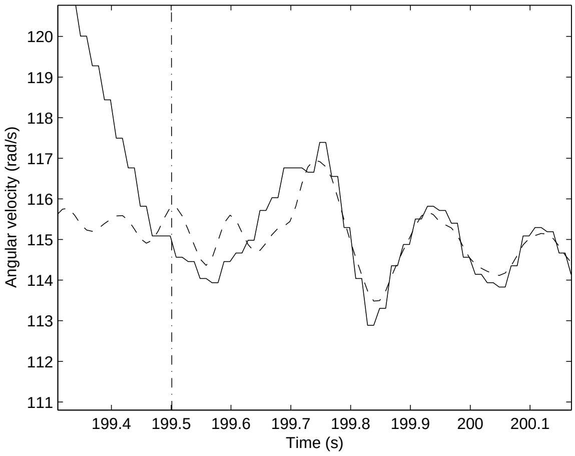

Figure 2.4. Engine speed (solid) and transmission speed (dashed) at the end of and right after a gear shift. The vertical line indicates when the gearbox goes from disengaged to engaged mode.

The moment of inertia of the final drive is neglected, which converts equation (2.9) to

$$T_f i_f = T_d, \quad \theta_p = \theta_f i_f \tag{2.16}$$

State Equations

The model is now simplified by putting the equations for the different parts together. Equations (2.1), (2.6), (2.10), (2.11), (2.14), (2.15) and (2.16) yield

$$\begin{aligned}(J_e + \frac{J_t}{i_t^2})\dot{\omega}_e &= T_{in} - (\frac{b_t}{i_t^2} + \frac{c_d}{i_t^2 i_f^2})\omega_e + \frac{c_d i_h}{i_t i_f}\omega_w \\ &\quad -\frac{k_d}{i_t i_f}(\frac{\theta_e}{i_t i_f} - \theta_w i_h) - \frac{T_{retarder}}{i_t}\end{aligned} \tag{2.17}$$

where $T_{in} = T_{comb} - T_{fr\ e} - T_{parasitic} - T_{exh}$. The equations (2.10), (2.11) and (2.13) yield

$$\begin{aligned}(J_w + mr_w^2)\dot{\omega}_w &= \frac{c_d i_h}{i_t i_f}\omega_e - c_d i_h^2 \omega_w \\ &\quad + k_d i_h(\frac{\theta_e}{i_t i_f} - i_h\theta_w) - T_{dr}\end{aligned} \tag{2.18}$$

Here, k_d includes the stiffness of both the propeller shaft and the drive shaft connected in series. The friction parameter c_d also includes the damping of both the shafts. The value of the new parameters can be obtained by using the formula for serial connection of stiffnesses, that is

$$k_d^{reduced\ model} = \frac{k_p i_f^2 k_d^{old}}{k_p i_f^2 + k_d^{old}} \tag{2.19}$$

The new friction coefficient c_d can be calculated in the same way. Now, the complete model of the engaged driveline can be written as a state-space model with the three states

$$\begin{aligned} x_1 &= \omega_e \\ x_2 &= \omega_w \\ x_3 &= \frac{\theta_e}{i_t i_f} - i_h \theta_w \end{aligned} \tag{2.20}$$

Equations (2.17) and (2.18) together with (2.20) yield

$$\begin{aligned} (J_e + \frac{J_t}{i_t^2})\dot{x}_1 &= T_{in} - (\frac{b_t}{i_t^2} + \frac{c_d}{i_t^2 i_f^2})x_1 \\ &\quad + \frac{c_d i_h}{i_t i_f} x_2 - \frac{k_d}{i_t i_f} x_3 - \frac{T_{retarder}}{i_t} && (2.21) \\ (J_w + m r_w^2)\dot{x}_2 &= \frac{c_d i_h}{i_t i_f} x_1 - c_d i_h^2 x_2 \\ &\quad + k_d i_h x_3 - T_{dr} && (2.22) \\ \dot{x}_3 &= \frac{x_1}{i_t i_f} - i_h x_2 && (2.23) \end{aligned}$$

which written on matrix form $\dot{x} = Ax + Bu$ gives

$$A = \begin{pmatrix} -\frac{(\frac{b_t}{i_t^2} + \frac{c_d}{i_t^2 i_f^2})}{(J_e + \frac{J_t}{i_t^2})} & \frac{\frac{c_d i_h}{i_t i_f}}{(J_e + \frac{J_t}{i_t^2})} & -\frac{\frac{k_d}{i_t i_f}}{(J_e + \frac{J_t}{i_t^2})} \\ \frac{\frac{c_d i_h}{i_t i_f}}{(J_w + m r_w^2)} & -\frac{c_d i_h^2}{(J_w + m r_w^2)} & \frac{k_d i_h}{(J_w + m r_w^2)} \\ \frac{1}{i_t i_f} & -i_h & 0 \end{pmatrix}$$

$$B = \begin{pmatrix} \frac{1}{(J_e + \frac{J_t}{i_t^2})} & -\frac{1}{i_t (J_e + \frac{J_t}{i_t^2})} & 0 \\ 0 & 0 & -\frac{1}{(J_w + m r_w^2)} \\ 0 & 0 & 0 \end{pmatrix}$$

where

$$\begin{aligned} u_1 &= T_{in} \\ u_2 &= T_{retarder} \\ u_3 &= T_{dr} \end{aligned} \tag{2.24}$$

2.2 Disengaged Driveline

The difference between the disengaged driveline and the engaged driveline is that the equations for the gearbox, (2.5) and (2.6), are no longer valid. The gearbox now instead divides the driveline into two different systems that work independently from each other. Since Opticruise never uses the clutch during an engine-controlled gear shift, the clutch always stays engaged. The first part of the driveline is the engine, the clutch and the ingoing shaft of the gearbox. Their speed is controlled by the engine torque. The second part includes the outgoing shaft of the gearbox, the shafts, the final drive, the hub reduction gear and the wheel.

Gearbox Disengaged

The inertia of the gearbox becomes divided into one part for each subsystem $J_{t,in}$ and $J_{t,out}$. The equations for the gearbox now yield

$$J_{t,in}\dot{\omega}_c = T_t - b_1\omega_c \tag{2.25}$$

$$J_{t,out}\dot{\omega}_t = -T_p - T_{retarder} - b_2\omega_t \tag{2.26}$$

Here b_1 and b_2 are the friction coefficients of the two parts.

2.2.1 State-Space Model for the Disengaged Driveline

By putting the equations for the different parts together, the model for the disengaged driveline is simplified in the same way as for the engaged driveline. Equations (2.1), (2.14) and (2.25) yield

$$(J_e + J_{t,in})\dot{\omega}_e = T_{in} - b_1\omega_e \tag{2.27}$$

The equations (2.10), (2.11), (2.15), (2.16) and (2.26) yield

$$\begin{aligned} J_{t,out}\dot{\omega}_t &= -(\frac{c_d}{i_f^2} + b_2)\omega_t + \frac{c_d i_h}{i_f}\omega_w \\ &\quad -\frac{k_d}{i_f}(\frac{\theta_t}{i_f} - i_h\theta_w) - T_{retarder} \end{aligned} \tag{2.28}$$

for the transmission speed, while the equations (2.10), (2.11) and (2.13) yield

$$\begin{aligned} (J_w + mr_w^2)\dot{\omega}_w &= \frac{c_d i_h}{i_f}\omega_t - c_d i_h^2\omega_w \\ &\quad +i_h k_d(\frac{\theta_t}{i_f} - i_h\theta_w) - T_{dr} \end{aligned} \tag{2.29}$$

for the wheel speed. The complete model of the disengaged driveline can now be written as a state-space model with the four states

$$\begin{aligned} x_1 &= \omega_e \\ x_2 &= \omega_t \\ x_3 &= \omega_w \\ x_4 &= \frac{\theta_t}{i_f} - i_h\theta_w \end{aligned} \tag{2.30}$$

Equation (2.27), (2.28) and (2.29) together with (2.30) yield

$$\begin{aligned}
(J_e + J_{t,in})\dot{x}_1 &= T_{in} - b_1 x_1 \\
J_{t,out}\dot{x}_2 &= -(\frac{c_d}{i_f^2} + b_2)x_2 + \frac{c_d i_h}{i_f}x_3 \\
&\quad -\frac{k_d}{i_f}x_4 - T_{retarder} \\
(J_w + mr_w^2)\dot{x}_3 &= \frac{c_d i_h}{i_f}x_2 - c_d i_h^2 x_3 \\
&\quad +k_d i_h x_4 - T_{dr} \\
\dot{x}_4 &= \frac{x_2}{i_f} - i_h x_3
\end{aligned} \tag{2.31}$$

which written on matrix form $\dot{x} = Ax + Bu$ gives

$$A_{disengaged} = \begin{pmatrix} -\frac{b_1}{J_e+J_{t,in}} & 0 & 0 & 0 \\ 0 & -\frac{\frac{c_d}{i_f^2}+b_2}{J_{t,out}} & \frac{\frac{c_d i_h}{i_f}}{J_{t,out}} & -\frac{k_d/i_f}{J_{t,out}} \\ 0 & \frac{\frac{c_d i_h}{i_f}}{J_w+mr_w^2} & -\frac{c_d i_h^2}{J_w+mr_w^2} & \frac{k_d i_h}{J_w+mr_w^2} \\ 0 & 1/i_f & -i_h & 0 \end{pmatrix} \tag{2.32}$$

$$B_{disengaged} = \begin{pmatrix} \frac{1}{J_e+J_{t,in}} & 0 & 0 \\ 0 & -\frac{1}{J_{t,out}} & 0 \\ 0 & 0 & -\frac{1}{J_w+mr_w^2} \\ 0 & 0 & 0 \end{pmatrix} \tag{2.33}$$

where u is the same as in equation (2.24).

2.3 Switching Between Engaged and Disengaged Mode

For reasons mentioned in section 2.1.1, a synchronization term between the engine and gearbox is included to deal with the difference in velocity that occurs after a gear shift. This will change the state equations and the transmission speed has to be introduced as a new state in the engaged driveline. To derive the new equations, equation (2.17) is divided by i_t. Together with the fact that $\omega_e = \omega_t i_t$ this yields

$$\begin{aligned}
(J_e + \frac{J_t}{i_t^2})\dot{\omega}_t &= \frac{T_{in}}{i_t} - (\frac{b_t}{i_t^2} + \frac{c_d}{i_t^2 i_f^2})\omega_t + \frac{c_d i_h}{i_t^2 i_f}\omega_w \\
&\quad -\frac{k_d}{i_t^2 i_f}(\frac{\theta_t}{i_f} - \theta_w i_h) - \frac{T_{retarder}}{i_t^2}
\end{aligned} \tag{2.34}$$

A new synchronization term, $(J_e + \frac{J_t}{i_t^2})d_{sync}(\omega_e - i_t\omega_t)$, is inserted in both equation (2.17) and (2.34) with the synchronization factor d_{sync}, which yields

$$\begin{aligned}
(J_e + \frac{J_t}{i_t^2})\dot{\omega}_e &= T_{in} - (\frac{b_t}{i_t} + \frac{c_d}{i_t i_f^2})\omega_t + \frac{c_d i_h}{i_t i_f}\omega_w \\
&\quad - \frac{k_d}{i_t i_f}(\frac{\theta_e}{i_t i_f} - \theta_w i_h) - \frac{T_{retarder}}{i_t} \\
&\quad -(J_e + \frac{J_t}{i_t^2})d_{sync}(\omega_e - i_t\omega_t) \qquad (2.35) \\
(J_e + \frac{J_t}{i_t^2})\dot{\omega}_t &= \frac{T_{in}}{i_t} - (\frac{b_t}{i_t^2} + \frac{c_d}{i_t^2 i_f^2})\omega_t + \frac{c_d i_h}{i_t^2 i_f}\omega_w \\
&\quad - \frac{k_d}{i_t^2 i_f}(\frac{\theta_t}{i_f} - \theta_w i_h) - \frac{T_{retarder}}{i_t^2} \\
&\quad +(J_e + \frac{J_t}{i_t^2})d_{sync}(\omega_e - i_t\omega_t) \qquad (2.36)
\end{aligned}$$

The states are now given as

$$\begin{aligned}
x_1 &= \omega_e \\
x_2 &= \omega_t \\
x_3 &= \omega_w \\
x_4 &= \frac{\theta_t}{i_f} - i_h\theta_w
\end{aligned} \qquad (2.37)$$

which written on matrix form $\dot{x} = Ax + Bu$ gives

$$A = \begin{pmatrix}
-d_{sync} & i_t d_{sync} - \frac{(\frac{b_t}{i_t} + \frac{c_d}{i_t i_f^2})}{(J_e + \frac{J_t}{i_t^2})} & \frac{\frac{c_d i_h}{i_t i_f}}{(J_e + \frac{J_t}{i_t^2})} & -\frac{\frac{k_d}{i_t i_f}}{(J_e + \frac{J_t}{i_t^2})} \\
d_{sync} & -i_t d_{sync} - \frac{\frac{b_t}{i_t^2} + \frac{c_d}{i_t^2 i_f^2}}{J_e + \frac{J_t}{i_t^2}} & \frac{\frac{c_d i_h}{i_t^2 i_f}}{J_e + \frac{J_t}{i_t^2}} & -\frac{\frac{k_d}{i_t^2 i_f}}{J_e + \frac{J_t}{i_t^2}} \\
0 & \frac{\frac{c_d i_h}{i_f}}{J_w + m r_w^2} & -\frac{c_d i_h^2}{J_w + m r_w^2} & \frac{k_d i_h}{J_w + m r_w^2} \\
0 & 1/i_f & -i_h & 0
\end{pmatrix} \qquad (2.38)$$

$$B = \begin{pmatrix}
\frac{1}{J_e + \frac{J_t}{i_t^2}} & -\frac{1}{i_t(J_e + \frac{J_t}{i_t^2})} & 0 \\
\frac{1}{i_t(J_e + \frac{J_t}{i_t^2})} & -\frac{1}{i_t^2(J_e + \frac{J_t}{i_t^2})} & 0 \\
0 & 0 & -\frac{1}{(J_w + m r_w^2)} \\
0 & 0 & 0
\end{pmatrix} \qquad (2.39)$$

with u given by (2.24). Although the synchronization term makes the model nonphysical, it is necessary if the engine and transmission speed are not to start deviating after each gear shift. If one were to look closely into this, it would probably be necessary to model the engagement and disengagement of the cogs as separate models. An advantage with having the transmission speed as a state in engaged mode, is that the model have the same states in the disengaged and in the engaged mode, which makes switching between the two Simulink models easier.

2.4 Simulation Environment

The models are implemented in Simulink and in appendix B an overview of the implementation is seen. All blocks are discrete since it is of interest to separate different samples. The equation solver is a discrete fixed step size solver. All input signals are considered to be constant between updates.

Chapter 3

Signals

The signals used in the driveline model described in chapter 2 are of different quality. There are both measured and estimated signals, which in turn have different sampling frequencies. The accuracy of the estimated signals also vary. In this chapter different aspects of the signal quality and their origins are described.

3.1 The Torques

According to the driveline model given in chapter 2, different torques are used as input to the driveline model. Here the different torques are described.

Engine Torque

The torque generated by the combustion, T_{comb}, comes from a formula where a certain injected fuel amount gives a certain torque. Approximate values are known for a specific engine, but may vary between different engines. At a static situation this is a fairly good estimation, but during transients the behavior is more uncertain. The signal is transmitted over the CAN-bus at a rate of 50 Hz.

Exhaust Brake Torque

The exhaust brake is a valve in the exhaust pipe which by stopping the exhaust flow increases the pump work of the engine, thus acting as a brake on the engine. The signal for actual exhaust brake torque, T_{exh}, has a low resolution. Modeling this torque in a simple and correct way is difficult, and therefore the signal can differ a lot from the actual exhaust brake torque. The value is transmitted over the CAN-bus at a rate of 20 Hz.

Engine Friction Torque

The engine friction torque, $T_{fr,e}$, can not be measured in a simple way. The value comes from a map based on engine speed and temperature and is estimated in the

Opticruise controller. The update frequency is 100 Hz.

Parasitic Losses

The parasitic losses are losses from external equipment as for example air conditioner, and the torque arising from this, $T_{parasitic}$, can not be measured easily. This signal is estimated using information about which external equipment that is currently used. The signal is received at a frequency of 4 Hz.

Retarder Torque

The retarder is a hydraulic brake used in trucks as a complement to the ordinary disc brakes. Since the maximum torque defined in production may differ with up to 10 % (according to [5]), the estimated retarder torque, which is based on the maximum retarder torque, is also uncertain. The retarder torque is measured and calculated by the Opticruise software and is therefore available in 100 Hz.

Drive resistance

The drive resistance torque T_{dr} collects all the torques generated by the air drag force, the rolling resistance and the slope of the road. It is estimated by the Opticruise software and is delayed due to filtering of the signal.

3.2 Velocities

Since the velocities are directly measured, they are in general of good quality compared to the estimated torque signals described above. Nevertheless, the problem with different update frequencies is existing here as well. A short description of the velocities follows.

Wheel Speed

The wheel speed is calculated as the mean speed of the two front wheels. The signal is given by the ABS-system which has a sensor on each wheel. Values of the mean front axle speed is transmitted over the CAN-bus at a frequency of 20 Hz.

Transmission Speed

There are two sensors measuring the rotational speed of the gearbox's output shaft, each giving a separate signal. The first comes from the tachograph which by law has to be installed in most trucks. The tachograph measures not only the speed of the gearbox's output shaft, but also how long time the vehicle has been moving or not moving. The tachograph signal is transmitted over the CAN-bus and comes with an update frequency of 25 Hz. The big disadvantage with this signal is that it is extensively filtered and therefore also time delayed with approximately 100 ms. The second signal comes from Opticruise's own sensor, which is directly connected to the control unit of the Opticruise system. This signal is available with an update frequency of 100 Hz and is of good accuracy. To begin with, the signal from the Opticruise sensor will be used. In chapter 10 a comparison between the use of the different sensors in the observer is made.

Engine Speed

The engine speed is measured on the output shaft of the engine. It is not measured by the Opticruise unit, but transmitted on the CAN-bus in 50 Hz. The accuracy is good.

3.3 State of the Gearbox

Since different models are used when the gearbox is engaged and disengaged, signals giving the actual state of the gearbox are needed as input to the model. These signals are assumed to be accurate and their update frequencies are 100 Hz.

Chapter 4

Parameters

The driveline model developed in chapter 2 contains a number of different parameters. In this chapter the parameters are described and the sensitivity of the driveline model with respect to the parameters is investigated. One method to estimate the damping and stiffness in the driveline and one method for estimating just the stiffness in the driveline is developed.

4.1 The Driveline Parameters

The parameters included in the model can be seen in table 4.1. The majority of these are mechanical parameters that can be measured or calculated from drawings. The moments of inertia can be calculated using for example a CAD-program. The transmission ratios and rolling radius are given from construction plans and the static torsional stiffness of all shafts can be measured. The total mass of the vehicle is a bit different, since it varies depending on how much load the vehicle is carrying. To start with, the mass is nevertheless looked upon as a given parameter.

4.2 Estimating Unknown Parameters

Since it is not possible to acquire all the needed parameters from technical data available at Scania, there is a need to estimate the values of the unknown parameters. These unknown parameters are the damping coefficient c_d, the friction coefficients b_i and the synchronization coefficient d_{sync}. Since the model is simple, the stiffness of the model's drive shaft probably captures more effects than just the stiffness in the real drive shaft, something which is also mentioned in [3]. Therefore it is also good if an on-line estimation of the stiffness is possible. There is reason to believe that the resulting stiffness and damping will vary with the gear engaged, since there is a stiffness in the clutch which will be transformed by the transmission ratio of the gearbox. Two different approaches to perform the estimations are investigated and will be described. None of the methods require any measurements of the torsion. The friction parameters, b_i, are further discussed

Parameter	Description
J_e	Moment of inertia of the flywheel and clutch.
J_t	Moment of inertia of the gearbox.
$J_{t,in}$	Moment of inertia of the gearbox acting on the input when in neutral gear.
$J_{t,out}$	Moment of inertia of the gearbox acting on the output when in neutral gear.
J_w	Moment of inertia of the wheels.
i_t	Transmission ratio of the gearbox.
i_f	Transmission ratio of the final drive.
i_h	Transmission ratio of the hub reduction gear.
k_d	Torsional stiffness of the drive shaft.
c_d	Internal damping coefficient of the drive shaft.
b_t	Damping coefficient of the gearbox.
m	Total mass of the vehicle.
r_w	Rolling radius of the wheel.
b_1	Damping coefficient of the gearbox input shaft when disengaged.
b_2	Damping coefficient of the gearbox output shaft when disengaged.
d_{sync}	Synchronization coefficient between the engine and transmission speed.

Table 4.1. Table of the parameters in the model

in the last part of this chapter and in chapter 8. The synchronization coefficient, d_{sync}, is tuned manually.

4.2.1 Estimation Using Integration of Angular Velocities

This approach is based on equation (2.10). The big problem with estimating k_d is getting a value of the drive shaft torsion, which cannot easily be measured. However, by integrating the difference in angular velocities between the transmission and wheel during a time interval, a measure of the change in torsion during the interval is achieved (see figure 4.1). Using this fact together with equation (2.10)

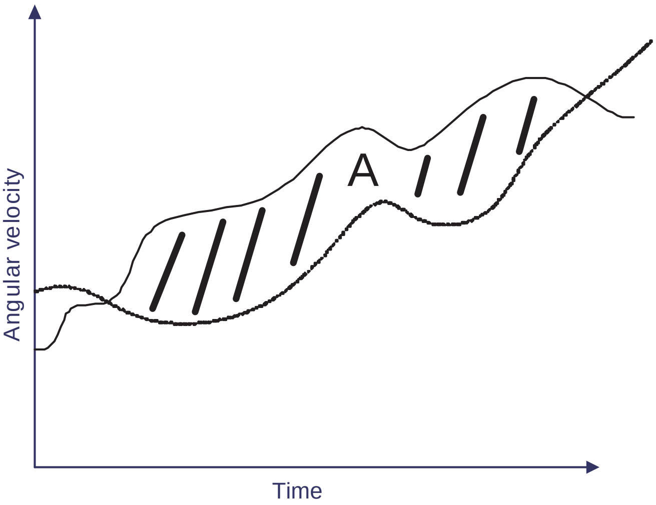

Figure 4.1. Angular velocities of the wheel and transmission scaled with the transmission ratios.

and taking the difference of this equation between the arbitrary times t_1 and t_2 yields

$$\begin{aligned} T_d(t_1) - T_d(t_2) &= k_d[(\theta_t(t1)/i_f - i_h\theta_w(t_1)) \\ &\quad - (\theta_t(t_2)/i_f - i_h\theta_w(t_2))] \\ &\quad + c_d[(\omega_t(t_1)/i_f - i_h\omega_w(t_1)) \\ &\quad - (\omega_t(t_2)/i_f - i_h\omega_w(t_2))] \end{aligned} \tag{4.1}$$

Choosing t_1 and t_2 such that the differences between the angular velocities are the same at both t_1 and t_2, i.e

$$\omega_t(t_1)/i_f - i_h\omega_w(t_1) = \omega_t(t_2)/i_f - i_h\omega_w(t_2) \tag{4.2}$$

and inserting that the torsion is equal to the area A, shown in figure 4.1. A is calculated by integrating the difference of the two signals between t_1 and t_2. Equation (4.1) is with the use of A simplified to

$$T_d(t_1) - T_d(t_2) = k_d A \tag{4.3}$$

where k_d is the only unknown parameter. Taking the difference between time points t_1 and t_2 in equation (2.13) and inserting equation (4.3) yields

$$(J_w + mr_w^2)(\dot{\omega}_w(t_1) - \dot{\omega}_w(t_2)) \quad = \quad k_d A - T_{dr}(t_1) - T_{dr}(t_2) \tag{4.4}$$

By approximating the angular acceleration with a backward difference and using (4.4), an estimation of k_d should be possible to calculate. To evaluate this, recordings of the signals are made with a Scania truck at the test course in Södertälje. However, the signals from both the angular velocities as well as from the driving resistance are too poor to get any probable values of the parameter. The biggest problem is integrating the difference in angular velocities, which by just having a small offset in the measurement, makes the torsion take on abnormal values. If better signals were available, foremost for the wheel speed, the estimation is believed to work.

4.2.2 Estimation Based on Oscillations in the Driveline

A second method to estimate the stiffness of the driveline is based on the oscillations that occur when going from and to neutral gear. One advantage of this method is that values are obtained for both the stiffness and the damping in the driveline. Theory and evaluation of the method follows.

Disengaged driveline

When the gearbox is put into neutral state, oscillations occur caused by the torque that is still present between the cogs in the gearbox. This procedure tries to identify the damping and frequency of the oscillations, and using the transfer function between one of the inputs $T_{retarder}$ or T_{dr} and one of the outputs ω_t or ω_w, an approximate analytical expression for the frequency and the damping is obtained. To begin with, the transfer function is derived from the state-space model for the disengaged driveline by using the formula

$$G(s) \quad = \quad C(sI - A)^{-1}B \tag{4.5}$$

where C is the matrix describing the measured signals. When the driveline is disengaged, the engine speed state is decoupled from the other states. Since the flexibility is between the gearbox and wheel, there is no need to take the engine speed into account. This means that only the last three states of the model have to be considered. Also, if only the transfer function from the driving resistance to the transmission speed is of interest, the following expressions can be used

$$A_{disengaged} = \begin{pmatrix} -\frac{\frac{c_d}{i_f^2}+b_2}{J_{t,out}} & \frac{\frac{c_d i_h}{i_f}}{J_{t,out}} & -\frac{k_d/i_f}{J_{t,out}} \\ \frac{\frac{c_d i_h}{i_f}}{J_w+mr_w^2} & -\frac{c_d i_h^2}{J_w+mr_w^2} & \frac{k_d i_h}{J_w+mr_w^2} \\ 1/i_f & -i_h & 0 \end{pmatrix} \tag{4.6}$$

$$B = \begin{pmatrix} 0 \\ -\frac{1}{J_w+mr_w^2} \\ 0 \end{pmatrix} \tag{4.7}$$

$$C = \begin{pmatrix} 1 & 0 & 0 \end{pmatrix} \tag{4.8}$$

By using (4.5), the system (4.6)-(4.8) and a symbolic handling software like Maple, the transfer function is calculated as

$$G(s) = \frac{(-i_h i_f c_d s - i_h i_f k_d)/(i_f^2 J_1 J_2)}{s(s^2 + c_d a s + k_d a)} \tag{4.9}$$

where

$$a = \frac{i_h^2 i_f^2 J_1 + J_2}{i_f^2 J_1 J_2}, \quad J_1 = J_{t,out}, \quad J_2 = J_w + mr_w^2. \tag{4.10}$$

This represents a third order differential equation with one real and two complex poles[1]. Assuming that the inputs are constant during the time right after neutral state is engaged, the dynamics of the system is determined by the homogeneous solution of the differential equation. The particular solution will in the case of a constant input only contribute with a constant solution. The homogeneous solution is given by the solution to the differential equation

$$\dddot{\omega}_t + c_d a \ddot{\omega}_t + k_d a \dot{\omega}_t = 0 \tag{4.11}$$

The solution to this equation, if all roots are simple, is according to [6]

$$\omega_t = C_1 e^{r_1 t} + C_2 e^{r_2 t} + C_3 e^{r_3 t} + C_4 \tag{4.12}$$

where r_i are the roots of the characteristic equation

$$r^3 + c_d a r^2 + k_d a r = 0 \tag{4.13}$$

which are calculated as

$$r_1 = 0 \quad r_{2,3} = -\frac{c_d a}{2} \pm i\sqrt{k_d a - \frac{c_d^2 a^2}{4}} \tag{4.14}$$

Since one root is zero, it only contributes to the solution by a constant. If the other two complex conjugated roots, are rewritten as a cosine and an exponential, the solution to (4.11) is

$$\omega_t = C_5 + C_6 e^{-\frac{c_d a}{2} t} \cos(\sqrt{k_d a - \frac{c_d^2 a}{4}} t + \phi) \tag{4.15}$$

---

[1] If the system oscillates it must have complex poles.

where ϕ is a phase shift and C_5 and C_6 are constants given by the boundary values. Introducing parameters for oscillation frequency ω_n and damping ζ as

$$\omega_n = \sqrt{k_d a - \frac{c_d^2 a^2}{4}} \tag{4.16}$$

$$\zeta = \frac{c_d a}{2} \tag{4.17}$$

equation (4.15) can be written as

$$\omega_t = C_5 + C_6 e^{-\zeta t} \cos(\omega_n t + \phi) \tag{4.18}$$

By looking at the oscillations that can be seen in figure 4.2, an identification of the parameters is possible. It is easy to visually identify the frequency of oscillation and equation (4.16) can then be used to estimate k_d and c_d. Since there are two unknown parameters, one more equation is needed. If the mean of the signal, i.e. C_5 and the constant coming from the particular solution are subtracted during the time interval of interest, the signal will be oscillating around zero. If the quotient of the signal value at two different maxima at time points t_1 and t_2 are compared, this yields

$$\frac{\omega_t(t_1)}{\omega_t(t_2)} = \frac{e^{-\zeta t_1}}{e^{-\zeta t_2}} \quad \Leftrightarrow \quad \zeta = \frac{1}{t_2 - t_1} \ln(\frac{\omega_t(t_1)}{\omega_t(t_2)}) \tag{4.19}$$

To use this, the mean of the signal during its oscillation is subtracted, and afterward the signal value as well as the time between two maximums is taken. By using the equations (4.16), (4.17) and (4.19), estimations of c_d and k_d are obtained as

$$c_d = \frac{2}{a(t_2 - t_1)} \ln(\frac{\omega_t(t_1)}{\omega_t(t_2)}) \tag{4.20}$$

$$k_d = \frac{\omega_n^2}{a} + \frac{c_d^2 a}{4} \tag{4.21}$$

Engaged Driveline

When a new gear is engaged oscillations visible in the engine and transmission speed occur. Using these oscillations the same estimation procedure can be made as for the disengaged driveline. By using

$$A = \begin{pmatrix} -\frac{c_d}{J_1 i^2} & \frac{c_d i_h}{i J_1} & -\frac{k_d}{J_1 i} \\ \frac{c_d i_h}{J_2 i} & -\frac{c_d i_h^2}{J_2} & \frac{k_d i_h}{J_2} \\ \frac{1}{i} & -i_h & 0 \end{pmatrix}$$

$$B = \begin{pmatrix} \frac{1}{J_1} \\ 0 \\ 0 \end{pmatrix}, C = \begin{pmatrix} 1 & 0 & 0 \end{pmatrix}$$

where $J_1 = J_e + \frac{J_t}{i_t^2}$, $J_2 = J_w + mr_w^2$ and $i = i_t i_f$, the transfer function is calculated by equation (4.5). This procedure yields the transfer function

$$G(s) \quad = \quad \frac{(J_2 s^2 + c_d i_h^2 s + k_d i_h^2)/J_1 J_2)}{s(s^2 + c_d a s + k_d a)} \tag{4.22}$$

where

$$a = \frac{i^2 i_h^2 J_1 + J_2}{i^2 J_1 J_2}$$

Since the denominator of equation (4.22) is exactly the same as for (4.9) with the exception that the parameter J_1 and therefore a is different, the same reasoning as above leads to the same equations, (4.20) and (4.21), for the estimations of the parameters in the engaged driveline.

Evaluation

A script is written in Matlab where an estimation of the parameters is made for every gear shift in a recording. The assumption that the input signals are constant during the oscillations is hard to validate, since a measurement of the driving resistance is not possible. However, since the driving resistance mainly depends on the vehicle speed and the slope of the road, and the wheel speed only changes a few percent during a gear shift, the assumption seem reasonable. A further problem is that the oscillations do not always occur and sometimes do not have the same appearance. This depends on how well zero torque in the gearbox i achieved at disengagement. Most of the oscillations are as the one seen in figure 4.2, which are in the range of 6-9 Hz. At times these oscillations can be very different, which can be seen in figure 4.3, where hardly any oscillations are visible. Taking this into account and just considering the oscillations which have basically the same appearance as the one in figure 4.2, values of k_d and c_d are obtained for the engaged and disengaged driveline.

For the engaged driveline the values of the parameters vary with the current gear engaged. More specific, the parameter values decrease with increasing gear. This is to be expected since the resulting stiffness and damping of two axes connected in series with a transmission in between is calculated as

$$k_{resulting} \quad = \quad \frac{k_1 i^2 k_2}{k_1 i^2 + k_2} \tag{4.23}$$

$$c_{resulting} \quad = \quad \frac{c_1 i^2 c_2}{c_1 i^2 + c_2} \tag{4.24}$$

where in this case k_1 is the clutch stiffness and k_2 is the stiffness in the propeller shaft, drive shaft and wheel combined. The transmission ratio is denoted i. The expressions (4.23) and (4.24) are strictly decreasing functions with regards to transmission ratio i, and since i decreases with increasing gear, k_d and c_d decrease with increasing gear. The method is evaluated with recordings from two different trucks, and in both cases values in a reasonable range are obtained. To compare

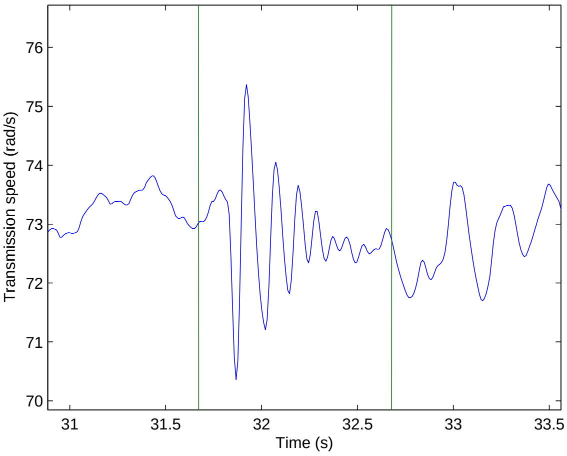

Figure 4.2. Oscillation in the transmission speed after engaging neutral gear. Vertical lines represents when neutral gear is engaged and disengaged.

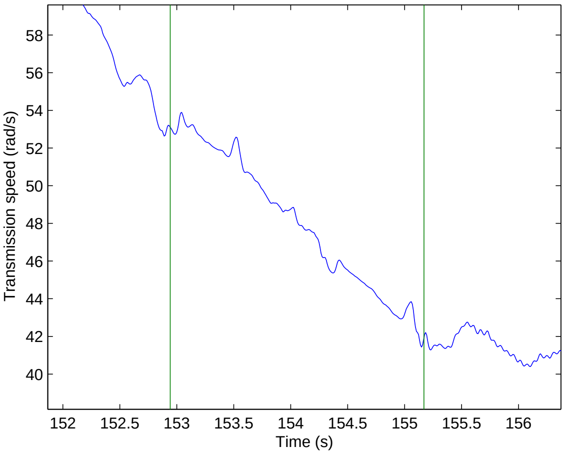

Figure 4.3. Oscillation in the transmission speed after engaging neutral gear. Vertical lines indicates engagement and disengagement of neutral gear.

the estimated parameters for the engaged driveline with the mechanical values equation (4.23) is rewritten as:

$$\begin{aligned} k_{resulting} &= \frac{1}{1/k_2 + 1/(i^2 k_1)} \Longleftrightarrow \\ 1 &= \frac{k_{resulting}}{k_2} + \frac{k_{resulting}}{i^2 k_1} \end{aligned} \tag{4.25}$$

Applying least squares method on equation (4.25) gives values of the parameters k_1 and k_2. Results from estimations of the stiffnesses in the two shafts for two different trucks (see appendix A for details about the trucks.) and the values taken from mechanical data are given in table 4.2 and 4.3.

	Estimations	Mechanical data
k_{clutch}	14100 Nm/rad	18500 Nm/rad
$k_{propeller,drive,wheel}$	118000 Nm/rad	103000 Nm/rad

Table 4.2. Stiffnesses in the clutch and propeller shaft, drive shaft and wheel combined from estimations and from mechanical data for the truck ”Melvin”

	Estimations	Mechanical data
k_{clutch}	15000 Nm/rad	37000 Nm/rad
$k_{propeller,drive,wheel}$	17300 Nm/rad	20000 Nm/rad

Table 4.3. Stiffnesses in the clutch and propeller shaft, drive shaft and wheel combined from estimations and from mechanical data for the truck ”Mastodont”

The mechanical value for the stiffness in the clutch is questionable since the clutch in reality is a highly non-linear spring. This makes the comparison between the values for this parameter uncertain and will not be discussed further. Looking at the value for the stiffness of the shafts and the wheel, the estimated values are accurate. There is however a difference to be expected, since the fact that only the propeller shaft, drive shaft and wheel have stiffnesses is an idealization.

For the disengaged driveline the estimations of the stiffness can be seen in table 4.4. The estimated value obtained in the disengaged driveline should describe the stiffness of the same part of the driveline as $k_{propeller,drive,wheel}$ does in the engaged driveline. As can be seen the estimated value for the disengaged driveline is almost a factor 10 smaller than $k_{propeller,drive,wheel}$ for the engaged driveline. Explanations for this difference have not been found.

	$k_{estimated}$
Melvin	16600 Nm/rad
Mastodont	3000 Nm/rad

Table 4.4. Estimated values o the stiffnesses in the case with a disengaged driveline.

The estimations for the engaged driveline give values of the stiffness which correspond well with the mechanical parameters. This can be seen as a sign that the estimation method works. The values for the disengaged driveline does however not correspond well with the mechanical parameters, but the model parameters are as previously mentioned expected to capture more effects than just the ones given from the mechanical parameters. Therefore, from these values it is hard to draw any more conclusions than that the values are of a reasonable magnitude and that the agreement between the mechanical and estimated values for the engaged driveline are promising. Validation of the parameters in a simulation with the driveline model can be seen in chapter 5.

4.2.3 Parameter Sensitivity of the Parameter Estimation

The estimation methods proposed in section 4.2 both include the mass of the vehicle and the moments of inertia of the engine, transmission and wheel. These parameters are not exactly known, which makes it interesting to know how sensitive the estimations are to faults in these parameters. However, the method in section 4.2.1 shows to be so sensitive to the signals that the method is not pursued any further. For the method proposed in section 4.2.2, a parameter sensitivity analysis is performed for the case with a disengaged driveline.

To get an overview of which parameters which influence the results of the estimations, an easy way is to vary the parameters in the estimations. A recording of the transmission speed from a Scania truck including a number of gear shifts is used. The parameters that are varied are the mass times the squared wheel radius (mr_w^2) and moments of inertia of the wheel and output shaft of the gearbox. The change relative a set value is then calculated and the results can be seen in table 4.5

Parameter	Change in parameter value	Change in estimated c	Change in estimated k
$J_{t,out}$	+10/-10%	+10/-10%	+9.82/-9.80%
mr_w^2	+10/-10%	0/-0.01%	0/-0.01%
J_w	+10/-10%	0/0%	0/0%

Table 4.5. Sensitivity of the parameter estimation with respect to different parameters

As can clearly be seen in table 4.5, the only parameter that play an important role in the estimation of the damping and the stiffness is $J_{t,out}$. This is a good result since this parameter is the same on all trucks and can be calculated with good accuracy. As previously described in section 4.2.2, the method with the engaged driveline ends up with exactly the same equations as for a disengaged driveline for the estimation except that J_1 and a are different. Since the estimation using a disengaged driveline is sensitive to the parameter J_1, and J_1 in the estimations in the engaged driveline is of the same magnitude, the method with the engaged driveline is sensitive to this parameter as well. This means that the parameter estimations are sensitive to J_e and J_t. These parameters are known with a good accuracy which makes the method insensitive to parameter variations.

4.3 Sensitivity Analysis of the Driveline Model

In this section the sensitivity of the driveline model with respect to its different parameters is examined. The parameters for moment of inertia of the engine and transmission, J_e and J_t are not considered since their values are calculated with good accuracy.

4.3.1 Differentiating the Driveline Model

One way to examine the parameter sensitivity of the model is to differentiate the equations with respect to the respective parameters. This is a very general procedure, and is recommended for simple systems. Nevertheless, doing this for the system described in chapter 2 yields large expressions which are hard to get a good overview of. The procedure is therefore not pursued further.

4.3.2 Simulating the Driveline

Given a driveline model with its parameters, it is easy to compare simulations with different parameters. By varying one parameter at a time, it is possible to see how much it influences the behavior of the system. If the behavior is more or less constant with respect to the parameter, the actual value of the parameter is not of great importance. However, if the behavior differs a lot, the value of the parameter has to be investigated in more detail. Plotting a spectrum of the signals, makes it easier to compare the frequency contents of the signals. To obtain a spectrum of the signals Welch's method is used, for further details see [9]. The plots presented in this chapter are mainly during a gear shift. The behavior for the engaged driveline model is however the same, wherefore plots are not shown.

Simulation Without Parameter Variations

In figure 4.4 the behavior of the transmission speed can be seen when no parameter variations are made. The first vertical line shows when the gearbox enters disengaged mode, and the second vertical line shows where the gearbox enters engaged mode. In figure 4.5-4.13 it is possible to see what happens to the simulated transmission speed when applying changes to the different parameters.

Increasing the Shaft Stiffness with 50%

Varying the stiffness in the drive shaft, k_d, has a great influence on the frequency of the oscillations when switching gear. In the frequency plot in figure 4.5, it can be seen that the peak frequency of the intensity has increased by 2 Hz. A closer look at the time domain plot shows that an increase in the stiffness only has minor influence on the damping of the oscillations. A change in the stiffness of the shaft can also clearly be seen by looking at the shaft torsion, see figure 4.6. A 50% increase in the parameter corresponds to a 50% scaling of the torsion. This means that if it is possible to measure the torsion, a very accurate estimation of the stiffness is believed to be possible. No measurement of the torsion has been

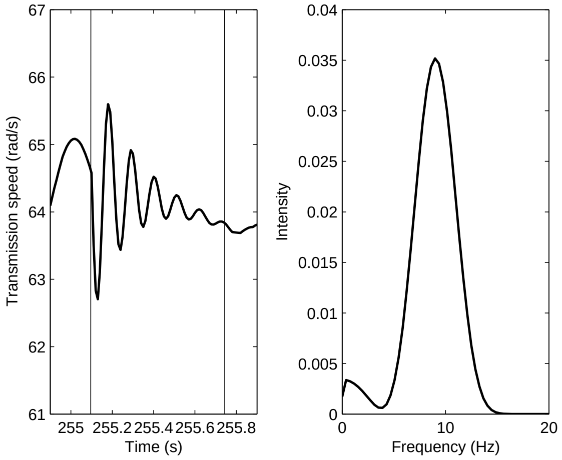

Figure 4.4. The transmission speed when simulating the system without any parameter variations. To the left: Transmission speed in the time domain. The gearbox is in neutral mode between the two vertical lines. To the right: Transmission speed in the frequency domain.

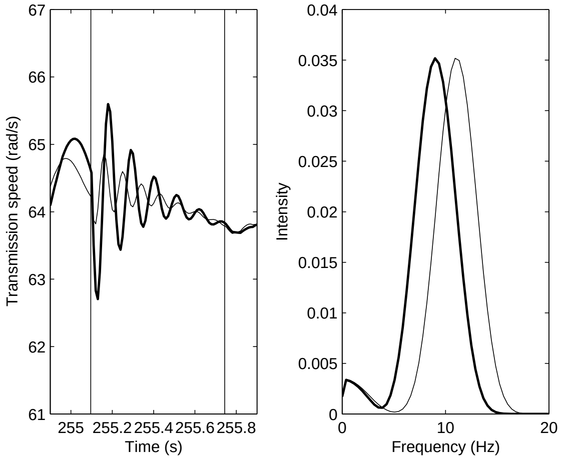

Figure 4.5. Increasing the stiffness by 50%. Bold line: The behavior of the system without variations. Thin line: The behavior of the system when the stiffness in the axes is increased by 50%. To the left: The transmission speed in the time domain. To the right: Transmission speed in the frequency domain

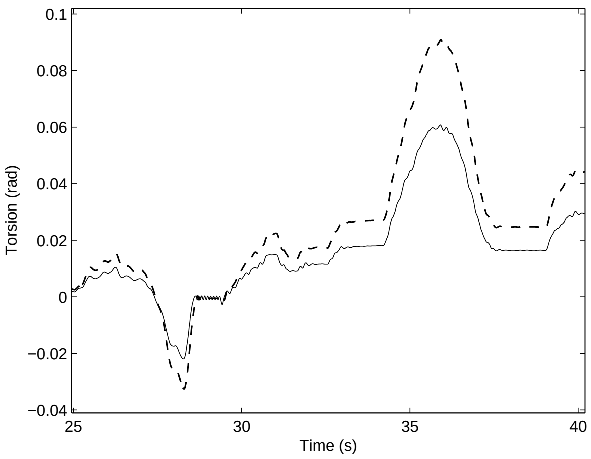

Figure 4.6. Shaft torsion with a change of 50% in the stiffness constant.

available during the course of this thesis. Further studies on estimations of this sort are therefore left as future work.

Increasing the Shaft Damping Coefficient with 50%

As can be seen in the frequency plot in figure 4.7, there are only minor changes of the frequency content of the transmission speed when the damping coefficient is increased by 50%. A certain change in the damping of the oscillations can nevertheless be seen in the time domain plot.

Increasing the Wheel's Moment of Inertia with 50%

Increasing the moment of inertia introduces no visible changes, see figure 4.8.

Increasing the Mass by 50%

Changing the mass by 50% has a great influence on the offset of the signal, which can be seen in figure 4.9. This means, that it is of a major importance to have an accurate value of the mass if the model is to estimate the behavior of the physical system correctly. The mass has nevertheless almost no influence on the frequency of the oscillation, see figure 4.9.

Increasing the Radius of the Wheel by 20%

Increasing the radius of the wheel by 20% has an influence on the system similar to the influence by changing the mass. Major offset changes occur as can be seen in figure 4.10. In the equation for the wheel the term

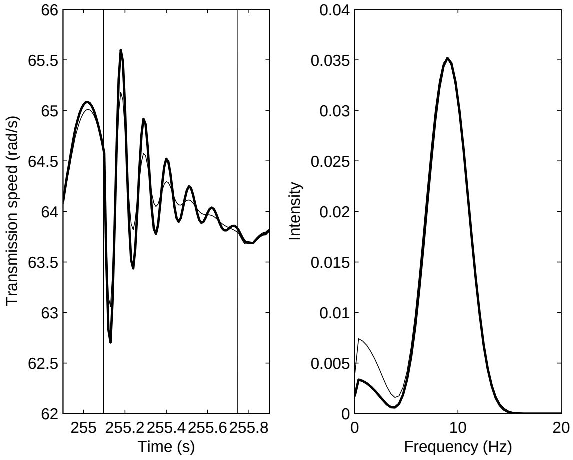

Figure 4.7. Increasing the damping by 50%. Bold line: The behavior of the system without variations. Thin line: The behavior of the system when the damping in the axes is increased by 50%. To the left: Transmission speed in the time domain. To the right: Transmission speed in the frequency domain.

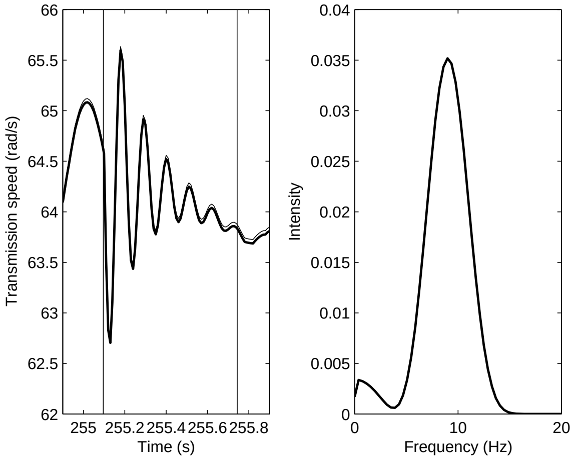

Figure 4.8. Increasing the moment of inertia of the wheel by 50%. To the left: Transmission speed in the time domain. To the right: Transmission speed in the frequency domain.

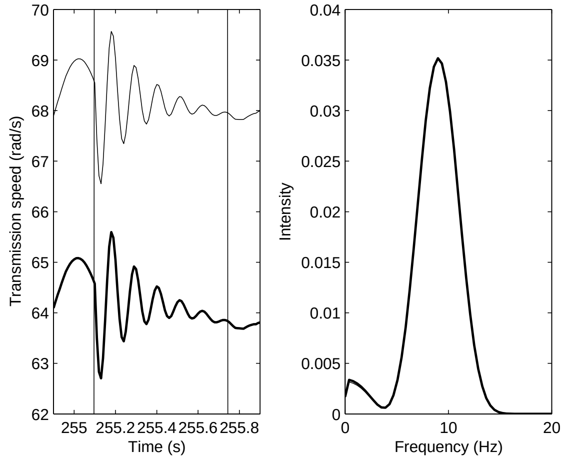

Figure 4.9. Increasing the mass of the truck by 50%. Bold line: The behavior of the system without variations. Thin line: The behavior of the system when the mass is increased by 50%. To the left: Transmission speed in the time domain. To the right: Transmission speed in the frequency domain.

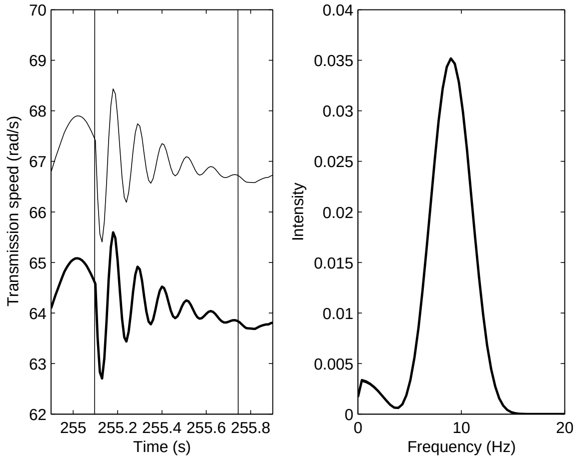

Figure 4.10. Increasing the radius of the wheel by 20%. Bold line: The behavior of the system without variations. Thin line: The behavior of the system when radius is increased by 20%. To the left: Transmission speed in the time domain. To the right: Transmission speed in the frequency domain.

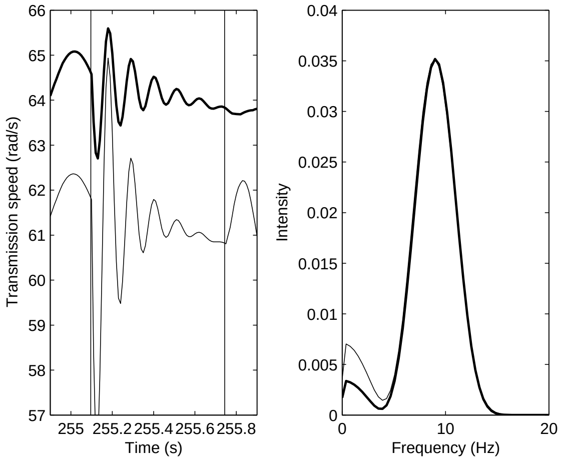

Figure 4.11. Increasing the friction coefficient b_t by 3 Nms/rad. Bold line: The behavior of the system without variations. Thin line: The behavior of the system when the parameters are increased. To the left: Transmission speed in the time domain. To the right: Transmission speed in the frequency domain.

$$\frac{1}{J_w + mr_w^2} \tag{4.26}$$

takes part. If the drive resistance is assumed to be very small, r_w only appears as in (4.26). Therefore, multiplying the mass by 1.5 (increasing the mass by 50 %), corresponds to an increase in the wheel radius by $\sqrt{1.5} \approx 1.22$ (22%). This means that a similar influence is expected for mass changes by 50% and for changes of the radius by 20%. Regarding the frequency contents, no changes can be seen in the frequency plot in figure 4.10.

Varying the Friction Coefficients

In the reference experiment, the friction coefficient b_t is set to zero. Increasing the coefficient by 3 Nms/rad has a great influence on the offset of the signal, which can be seen in figure 4.11. In figure 4.12 it can be seen that another possible result when increasing the parameters is that the two simulations start to diverge during a gear shift. Minor changes in the frequency contents can also be seen.

Increasing the Synchronization Coefficient

The synchronization coefficient, d_{sync}, describes how the engine speed and the transmission speed are synchronized when the gearbox switches from disengaged to engaged mode. Increasing this parameter can be seen as increasing the punishment for deviations between engine speed and transmission speed just after a gear shift. As shown in picture 4.13, increasing d_{sync} affects the amplitude of the

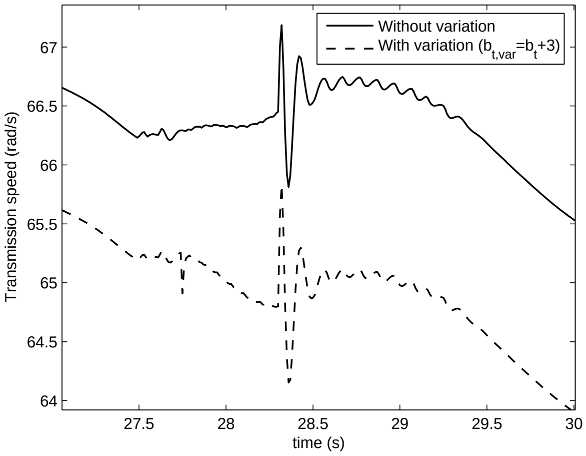

Figure 4.12. gear shift behavior when the damping coefficient b_t is incremented by 3 Nms/rad. Bold line: Reference experiment. Thin line: Experiment with varied parameters

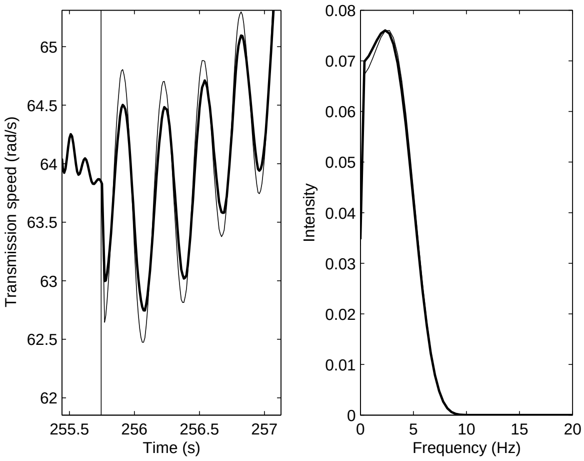

Figure 4.13. Increasing the synchronization coefficient d_{sync} by 50%. Bold line: The behavior of the system without variations. Thin line: The behavior of the system when radius is increased by 50%. To the left: Transmission speed in the time domain. To the right: Transmission speed in the frequency domain.

oscillations when going from disengaged to engaged mode. In the frequency plot in figure 4.13, the 50% increase in d_{sync} has almost no influence on the frequency of the oscillations that occur just after a gear shift.

4.4 Results and Summary

An estimation of the stiffness in the driveline using the method described in section 4.2.1 is not possible to perform because of poor signal quality. It is nevertheless possible to obtain values of the stiffness and the damping in the driveline using the method described in section 4.2.2. These values are promising, but simulations of the driveline are necessary to check if they also capture the correct frequency in the model. The fact that only two trucks are tested in this thesis is a further uncertainty, and more tests on different trucks are needed to check the functionality of the method. As is seen in the parameter sensitivity analysis, the frequency of the oscillations in the model directly correspond to the values of the stiffness and therefore these parameters must be estimated very precisely if the oscillations are to be captured correctly by the model. Simulations and validation with the estimated and mechanical parameters is further discussed in chapter 5.

The mass of the truck has the same effect as the moments of inertia in the model, and in comparison with the moment of inertia of the wheel, it has due to its high value on a truck a much higher impact on the model. Worth to notice is that a 50% deviation of the mass of the vehicle or a 20% deviation of the radius of the wheel, changes the offset of the transmission speed immensely. This implies the significance of having accurate values for these parameters. The wheel radius also affect the wheel speed, which must be transformed from the speed of the vehicle. This will show more clearly when a Kalman filter is designed for the model. The friction coefficient b_t makes a significant difference, but from numerous trials with variations of this parameter, it has been shown that any value of this parameter does not improve the behavior of the model in comparison to setting it to zero.

To summarize, it is shown that the mass and wheel radius are important in order to remove bias errors. Concerning the oscillations, the main focus is on the stiffness and damping coefficient of the drive shaft. The moment of inertia of the wheel and the synchronization coefficient does however not play an important role.

Chapter 5

Simulation and Validation of the Driveline Model

In this chapter the model is validated against the measured speed signals of the engine, the output shaft of the gearbox and the wheel. The difference between using the estimated shaft stiffness and the stiffness obtained from mechanical data is also investigated. To validate the model, recordings of the interesting signals with two Scania trucks are used.

5.1 Simulations Using Recordings from the Truck ”Mastodont”

The first truck available is ”Mastodont” (for details about this truck, see appendix A). No trailer is used at the test run, which makes the truck light (approximately 10 tons). The truck is equipped with hub reduction gear making the driveline stiff, which in combination with the absence of a trailer makes small oscillations to be expected. Parameters are taken from mechanical data and from estimations previously described. The results of the first recording for all states of the model can be seen in figure 5.1 and 5.2.

The agreement between the measured and simulated signals are good considering the poor quality of some of the input values. The main dynamics are captured and the offset is not disturbingly big. By using a feedback with the measured values, the offset should be possible to eliminate. The estimated torsion is hard to validate since no measured signal is available. The values are nevertheless reasonable and in the same range as values seen in similar papers, like in for example [8]. A close-up on the engine and transmission speed during a gear shift can be seen in figure 5.3. Here the agreement is good considering the simplicity of the model and that the model is not specialized just for the gear shift. The frequency of the oscillations seem to be fairly accurate making the estimation method for the stiffness promising.

A second gear shift can be seen for the transmission speed in figure 5.4. Here

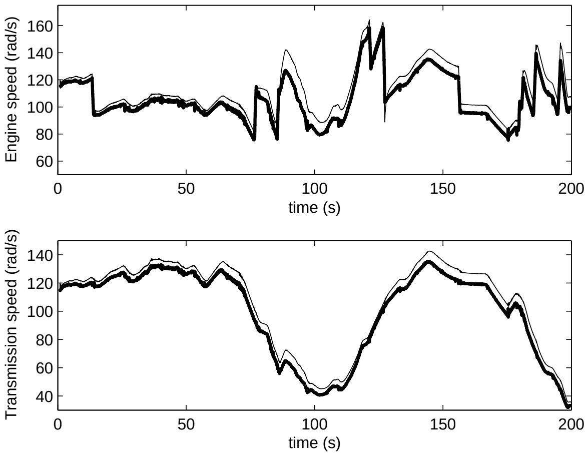

Figure 5.1. Simulated (thin) and measured (bold) engine and transmission speed.

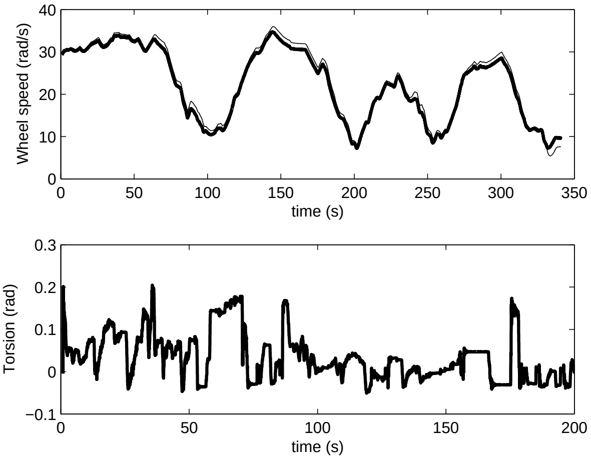

Figure 5.2. Simulated and measured (bold) wheel speed, simulated torsion in the drive shaft.

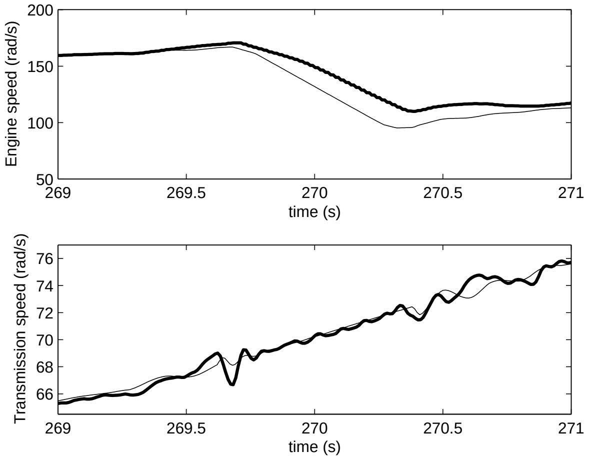

Figure 5.3. Simulated (thin) and measured (bold) engine and transmission speed during a gear shift.

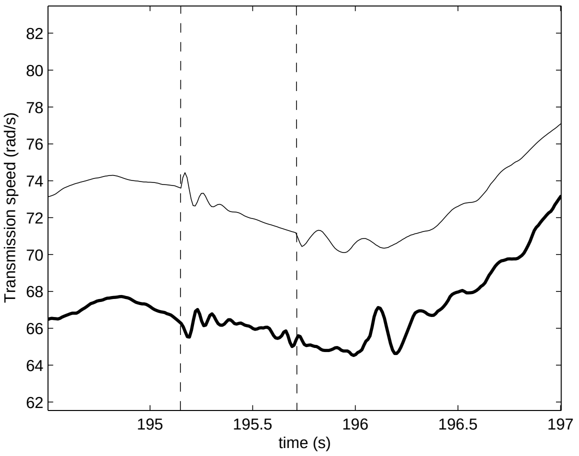

Figure 5.4. Simulated (thin) and measured (bold) transmission speed during a gear shift. Vertical dashed lines represents the signal indicating neutral gear.

the oscillations of the transmission speed can be seen to start in the opposite direction compared to the measurements. A probable explanation to why some oscillations start in the opposite direction and some don't, is that the actual torsion at the moment of decoupling is acting in the opposite direction compared to the estimated torsion. Partly this is caused by the inaccuracy in the signal indicating when the gearbox goes into neutral gear. This problem is hard to solve since no better signal is available, and since the torsion is almost zero at this point a small error in the torsion makes a big difference. Another problem is that the oscillations that occur at the engagement of the new gear start too early. This problem does not occur at every gear shift, making it hard to tackle.

Some oscillations that occur after a gear shift might also be caused by a so called backlash in the driveline. The backlash is caused by the gaps between the cogwheels. Because the engine and the propeller shaft are not really connected, oscillations at close-to-zero torque are difficult to predict. Another factor to take into consideration here is the nonlinearity of the coupling, which at close to zero torsion have very soft springs.

If the torque crosses zero, oscillations will occur in the driveline, but since the backlash is not modeled they do not occur in the modeled angular velocities.

A second recording is used to validate the model and the result can be seen in figure 5.5. Here the main dynamics are still captured but the offset increases with time. This is of course troubling, but after discussion with some staff at Scania, the cause likely lies in an overestimation of the engine friction torque, which in turn makes the signals slump. A feedback with the measured signals based on Kalman theory can hopefully take care of this problem.

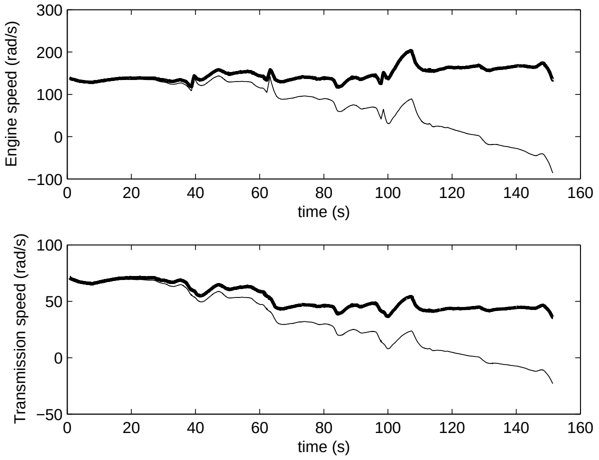

Figure 5.5. Simulated (thin) and measured(bold) engine and transmission speed.

5.2 Simulations Using Recordings from the Truck ”Melvin”

The second truck used for validation is ”Melvin” (for details see appendix A), which at the test run was weighing approximately 20 tons. The driveline is not as stiff as for ”Mastodont”, and therefore oscillations with larger amplitude are to be expected.

The results for the transmission and engine speed from this recording and simulation can be seen in figure 5.6. Here it can be seen that both simulated signals oscillate with a too small damping when the driveline is engaged. During a gear shift the frequency and damping seem more accurate, which can be seen for the transmission speed in figure 5.7. Since the estimated damping seem to be too low it is increased by a factor ten and a result from a simulation can be seen in figure 5.8. Here the estimated transmission speed signal capture the oscillations with a correct frequency.

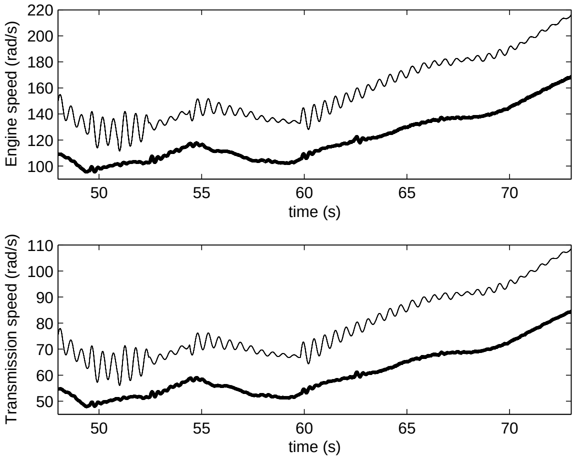

Figure 5.6. Simulated (thin) and measured (bold) engine and transmission speed.

To validate if the frequency is correct, a spectrum of both the measured and estimated signal is produced. To be able to see the first mode of oscillation the signals are first high pass filtered with a low break frequency. The spectra can be seen in figure 5.9, and the model seem to capture the first mode of oscillation relatively correct. Achieving a good spectrum for the measured signal, showing the first mode of oscillation has proved hard, since disturbances in the same frequency range occur. A close look at the time plots for both the measured and estimated transmission speed signal show that the interesting frequency lies at approximately 2.5 Hz for both signals in figure 5.8.

As could be seen in section 4.2.2 there is no big difference between the values for

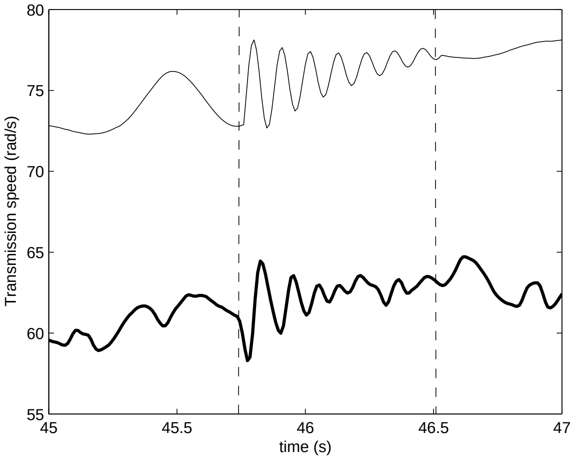

Figure 5.7. Simulated (thin) and measured (bold) transmission speed during a gear shift. Vertical dashed lines represent engagement and disengagement of neutral gear.

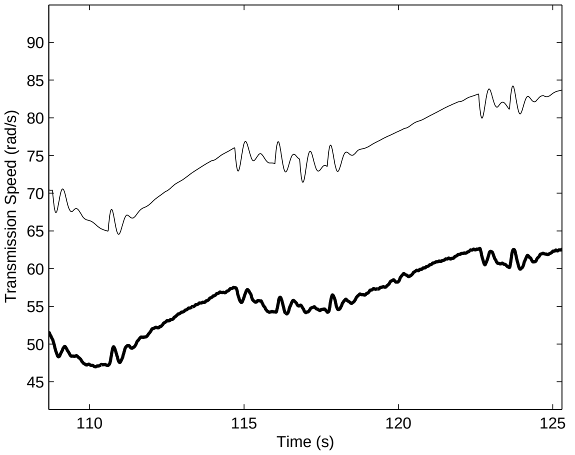

Figure 5.8. Simulated (thin) and measured (bold) transmission speed.

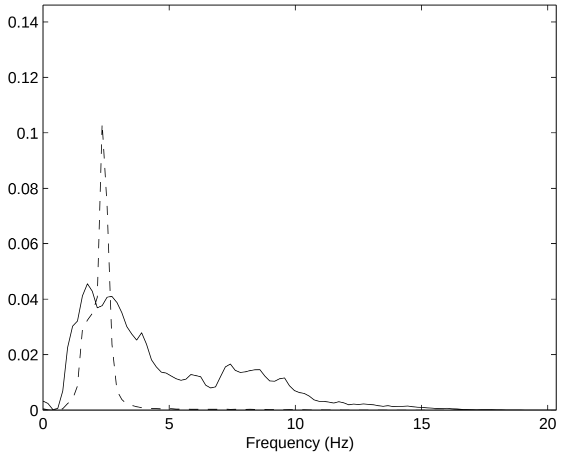

Figure 5.9. Power spectrum of the measured (solid) and simulated transmission speed (dashed).

the mechanical and estimated parameters of the stiffness for an engaged driveline. In figure 5.10 a comparison between the estimated transmission speed with the estimated and mechanical stiffness is seen. As expected there is no big difference and the frequency is just slightly higher. In this thesis the focus is to achieve smooth signals at a rate of 100 Hz, and the ability to capture the oscillations exactly correct is not considered top priority. As has been shown here, no big difference is achieved from estimating the stiffness for the engaged driveline. For the disengaged driveline the estimated stiffness is however significantly different from the mechanical values. Since the estimated values show good property during the gear shifts these are preferred.

One problem is that the model does not capture all oscillations due to unmodeled phenomenas as for example the backlash previously mentioned. Another problem is that the oscillations sometimes start at the wrong time point. This is believed to originate from flaws in the input signals.

To summarize, the model captures the big dynamics of the system with an offset that might increase over time. Trials with different simulation speeds have shown that it is possible to simulate at approximately 250 Hz, which is too slow. The estimated stiffnesses show relatively good results, and for the applications in this thesis they are considered accurate enough. The estimated damping is however too small and therefore the damping has to be more or less guessed to suit the truck. The fact that the value of the damping is too small, makes the value of the stiffness questionable considering that the damping value is needed to calculate the stiffness, see equations (4.20) and (4.21). Further investigations into this are not given in this thesis.

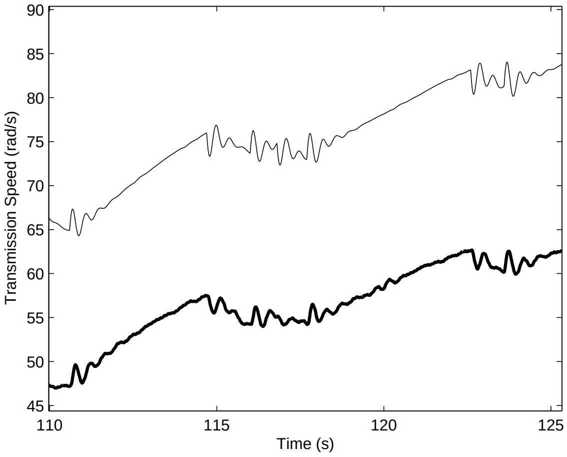

Figure 5.10. Simulated (thin) and measured (bold) transmission speed.

Chapter 6

Basic Theory for the Observer

In this chapter basic theory for the system and the observer is discussed. This includes theory for discretization and Kalman filtering. This chapter is based on parts from [7] and [9]. The Kalman filter is an observer which includes a model of the system.

6.1 Discretization

The measured signals are sampled with different sampling frequency, and the available new information will therefore differ between sample points. In order to take this into account, the continuous time model has to be transformed into a time discrete model instead. Since the inputs are considered constant between sample points, the best possibility is to sample the system, see for example [7].

The model in this thesis is implemented in Simulink which approximates the derivatives in order to discretize the model. Therefore an approximation of the derivatives is used when making the model discrete. There are several ways to perform this approximation and the easiest method is the Euler approximation given by

$$\dot{x}(t) = \frac{x(t+T) - x(t)}{T} \tag{6.1}$$

where T is the sample period. A better approximation is however the so called Tustin's formula

$$p = \frac{2}{T}\frac{q-1}{q+1} \tag{6.2}$$

where p stands for the derivation operator and q for the delay operator.

6.2 Observer and Kalman Filtering

Normally not all states in a system can be measured. The problem is to estimate the states with help from the available measured signals. There are fundamental limitations to the observability of all states. For a linear system where A is an $n \times n$ matrix, the observability matrix can be calculated as

$$O(A, C) = \begin{bmatrix} C \\ CA \\ \vdots \\ CA^{n-1} \end{bmatrix} \tag{6.3}$$

and all the states are observable if and only if O has full rank. This does however give no information about how good the estimations in practice will be.
A linear time invariant discrete time system can be written on the form

$$\begin{aligned} x(t+T) &= Ax(t) + Bx(t) + Nv_1(t) \qquad (6.4) \\ y(t) &= Cx(t) + v_2(t) \qquad (6.5) \end{aligned}$$

where v_1 is the process noise, v_2 is the measurement noise and T is the sample time. A first approach to estimate the states is to simulate the system using only the known input values:

$$\hat{x}(t+T) = A\hat{x}(t) + Bu(t) \tag{6.6}$$

To measure the quality of the simulation, the difference $y(t) - C\hat{x}(t)$ can be used. If the model and signals are perfect this would equal zero, but since there are always some model errors and disturbances this is not the case.

A good way to improve the estimations is to use $y(t) - C\hat{x}(t)$ as a feedback signal in the simulation such that

$$\hat{x}(t+T) = A\hat{x}(t) + Bu(t) + K(y(t) - C\hat{x}(t)) \tag{6.7}$$

The value of K becomes an adjustment between how fast the estimations converge toward the measurement and how sensitive the estimation is to measurement noise, see for example [7] and [9]. A schematic picture of the filter can be seen in figure 6.1.

The Kalman filter is equation (6.7) together with the K that minimizes the variance of the error in the state estimation, i.e. $x(t) - \hat{x}(t)$. This can be calculated from the equation

$$K = (APC^T + NR_{12})(CPC^T + R_2)^{-1} \tag{6.8}$$

where P is calculated from the stationary Riccati equation:

$$\begin{aligned} P = {} & APA^T + NR_1N^T - (APC^T + NR_{12}) \\ & \times (CPC^T + R_2)^{-1}(APC^T + NR_{12})^T \end{aligned} \tag{6.9}$$

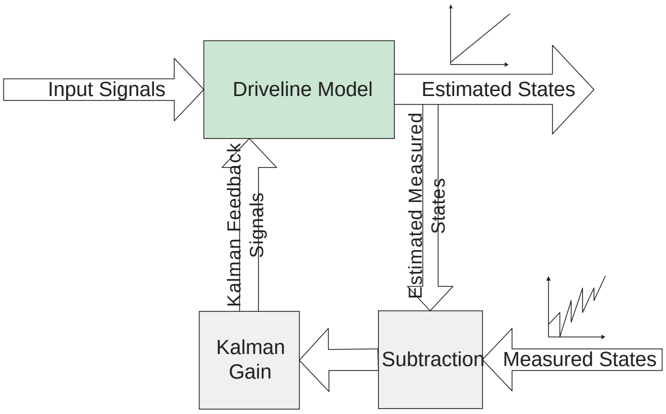

Figure 6.1. Schematic picture of the Kalman filter.

R_1 and R_2 are the intensities of the white process noise v_1 and the white measurement noise v_2. P is also equal to the covariance matrix of the optimal estimation error $x(t) - \hat{x}(t)$. R_{12} is the constant cross spectra between v_1 and v_2.

The process noise of the driveline model is believed to mainly originate from model inaccuracies and inaccuracies in the estimated input signals to the model, whereas the measurement noise arise from sensor vibrations etcetera. No connection between the two kinds of noise is believed to be probable, which yields R_{12} equal to zero. From now on, R_1 and R_2 are denoted Q and R. In the design of the Kalman filter the quotient between Q and R is the design parameter, the absolute values do not matter, see [9]. A larger Q means a bigger trust in the measurements which at the same time makes the observer more sensitive to measurement noise. On the other hand, a smaller Q puts more trust in the model and therefore makes the observer more sensitive to process noise and model errors.

6.3 Calculating the Covariance Matrices

The noise of the system is divided into two groups called process and measurement noise. The process noise is the disturbances that occur on the driveline, that is on the inputs to the driveline or due to modeling errors. The measurement noise is the disturbances on the signals from the sensors that measure the interesting signals used for feedback. From a control perspective the goal is to control the process noise without being fooled by the measurement noise.

The observer is influenced by both measurement noise and process noise. By investigating the measured signals, it is possible to obtain an estimation of the relationships in the covariance matrix R and Q used in section 6.2. Assume, just for this section, that the measurement noise is of high frequency character and therefore can be characterized by

$$v = \bar{y} \tag{6.10}$$

where $\bar{y}$ is the high-pass filtered measured signal. The process noise can be estimated in a similar way for the states that are measurable. By assuming, just for this section, that the process noise is of low frequency character it can be introduced as

$$w = f(\hat{x}, u) - \dot{\bar{x}} \tag{6.11}$$

where $\dot{\bar{x}}$ are the low-pass filtered and differentiated measured states, and $f(\hat{x}, u)$ are differentiated estimated states. Differentiation of the measured states $\bar{x}$ is done with a non-causal central differentiation filter. There is no need to differentiate the estimated states, since the derivatives already exist in the Simulink model.

The elements of R and Q can now be calculated as

$$\hat{R}_{ij} = \frac{1}{N} \sum_{t=1}^{N} v_i(t) v_j(t) \tag{6.12}$$

$$\hat{Q}_{ij} = \frac{1}{N} \sum_{t=1}^{N} w_i(t) w_j(t) \tag{6.13}$$

Here, i and j denotes the index of the measured signals and N is the length of the data sequences. The estimation of the covariance matrix R and Q according to equations (6.12) and (6.13) can be performed in MATLAB using the command `covf`.

6.4 Motivating the Use of a Kalman Filter

The Kalman filter is a stochastic filter that assumes all disturbances to be stochastic a priori known variables. If the system is linear and both the process and measurement disturbances have a normal distribution it can be shown that the Kalman filter is also the optimal filter [9].

If the noise of the measured signals is assumed to be of a high frequency character just like in the previous section, high pass filtering the transmission speed yields an approximation of the measurement noise. This procedure is mainly motivated by the fact that the desired information in the signals is of low frequency character and therefore non of this information is included in the calculations of the covariances. In figure 6.2 a histogram over this transmission speed noise is given. The data sequence is taken in the case of an disengaged driveline where the engine does not affect the transmission speed. As can be seen in the figure, the distribution seem to approximate a normal distribution, which motivates the use a Kalman filter.

Similar plots can be shown for the process and measurement noise described in section 6.3. This is no evidence that the disturbances are gaussian, it rather makes an assumption concerning this plausible.

There are deterministic counterparts to the Kalman filter like the Robust filter. In this thesis only the Kalman filter is tested, but in [10] a comparison between the different filter types are made. Since the Kalman filter is the optimal filter for a linear system with gaussian noise, it has be chosen for this thesis.

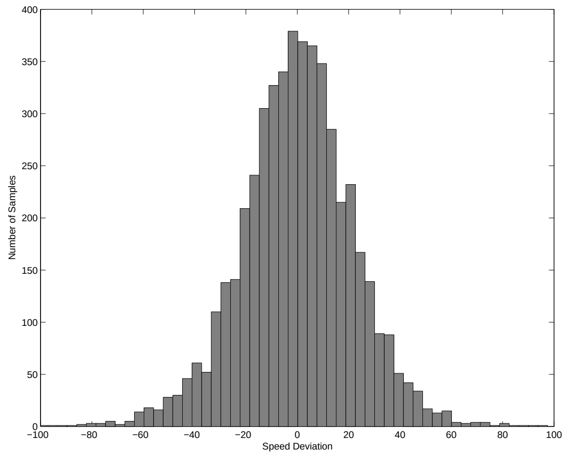

Figure 6.2. Distribution of the transmission speed noise.

6.5 Extending the Model with Noise States

In an observer it is desirable to have all disturbances as white noise, i.e. a random signal with constant spectrum. In general the noise is however not white, but consists of certain frequencies. In theory, if the spectrum of a signal is known, the signal can be described as the output of a filter driven by white noise. Using this, a model with non-white noise can be extended with new noise states, so that all noise is white. The problem now lies in describing the noise signal as a filter driven by white noise. If a filter describing the noise is found, it can be written on a state-space form and included in the original state-space system. Consider a system given on the form

$$\dot{x}_a = A_a x_a + B_a u_a + N_a v_a \tag{6.14}$$
$$y = C_a x_a + n \tag{6.15}$$

where v_a is white noise representing system noise and n is the measurement noise which is not white noise. If we are able to describe n as the output of a filter on the form

$$\dot{x}_n = A_n x_n + B_n v_2 \tag{6.16}$$
$$n = C_n x_n + D_n v_2 \tag{6.17}$$

then combining (6.17) with (6.15) gives the new state-space system

$$\dot{x} = Ax + Bu + Nv_1 \tag{6.18}$$
$$y = Cx + v_2 \tag{6.19}$$

where

$$x = \begin{bmatrix} x_a \\ x_n \end{bmatrix}, \qquad v_1 = \begin{bmatrix} v_a \\ v_2 \end{bmatrix}, \qquad A = \begin{bmatrix} A_a & 0 \\ 0 & A_n \end{bmatrix} \tag{6.20}$$

$$B = \begin{bmatrix} B_a \\ 0 \end{bmatrix}, \quad N = \begin{bmatrix} N_a & 0 \\ 0 & B_n \end{bmatrix}, \quad C = \begin{bmatrix} C_a & C_n \end{bmatrix} \tag{6.21}$$

and v_1 and v_2 is white noise. The same procedure can be used for the process noise.

Chapter 7

Observer Design

The model described in the previous chapters is used in a Kalman filter to improve the performance of the observer. The feedback used in a Kalman filter makes the system more stable and simulations in 100 Hz are possible. Problems with the observer are discussed, and last in this chapter an estimation of the rolling radius is extracted from the observer.

7.1 Observability of the Model

All the states in the engaged driveline model are observable when measuring at least the transmission speed, which can be shown using the observability criterion (6.3). Measuring additional signals like the engine and wheel speed will not affect the observability in a negative way. The engine speed state is not observable in decoupled mode if only the transmission or wheel speed is measured. This is natural since there is no connection between the transmission/wheel speed and the engine speed in neutral mode. In this case, measuring at least the engine and transmission speed makes the model observable.

7.2 Designing the Observer

This first design of the observer assumes that all measurement disturbances are white. A further assumption is that the process noise is given by model uncertainties which in turn are white. The systems described by the matrices (2.32), (2.33), (2.38) and (2.39) are made discrete by using the methods described in section 6.1. To these systems white measurement noise and system noise, describing model inaccuracies, are added with intensities Q and R calculated as described in section 6.3. The quotient between Q and R is scaled with a constant factor to influence the design of the filter gain. The system is now written on the form

$$x(t+T) = Ax(t) + Bu(t) + Nv_1(t) \tag{7.1}$$

$$y(t) = Cx(t) + v_2(t) \tag{7.2}$$

where N is chosen as

$$N = \begin{pmatrix} 1 & 0 & 0 \\ 0 & 1 & 0 \\ 0 & 0 & 1 \\ 0 & 0 & 0 \end{pmatrix} \tag{7.3}$$

With help from the Matlab command `dlqe` equation (6.9) is solved. Using this solution and equation (6.8) the Kalman gain is calculated. Different values of the scale factor of the quotient between Q and R are tested, and the result of the best choice considering both bias and noise sensitivity can be seen in section 7.4.

Due to the nature of the system, different Kalman gains are calculated depending on which gear that is currently engaged or if the gearbox is in neutral gear. There are also different number of measured signals available at different sample points. To deal with this, different Kalman gains are calculated depending on which signals that hold new information at the current sample. By changing the C-matrix in (7.2) and using the method described earlier to calculate the Kalman gain this is achieved. Updating the three different signals (engine speed, transmission speed and wheel speed) at different rates, require that there are four different feedback matrices for each gear, including the neutral state[1]. The trucks used in this work all have 14 gears and a neutral state, and this means that using this method there is a need for 60 different Kalman gains. No use of theory for time varying system matrices is used here, since its use is believed to be too computationally demanding.

7.3 Implementation

The Simulink implementation of the driveline model is extended with a Kalman filter, using the measurements of the engine, transmission and wheel speed as input to the Kalman filter. An overview of the implementation is seen in appendix B.

7.4 Evaluation

To evaluate this first approach of the observer, a test run with the truck "Melvin" is used. A short section from the simulations can be seen in figure 7.1. As can be seen from the plots of the speed signals, small bias errors are present. Their occurrences are mainly located at times when truck goes from acceleration from retardation, see more under item 2 below. The behavior of the system is, with exception of the faults given below, satisfactory. Not all of these faults can be seen in the figure.

The problems identified while looking closely at the simulations with the Kalman filter and some of the input signals are as follows:

1. **Inaccurate acceleration and deceleration of the engine speed during a gear shift:** This problem occurs both during an up shift and down

---

[1] There are only four matrices since the transmission speed is measured every sample

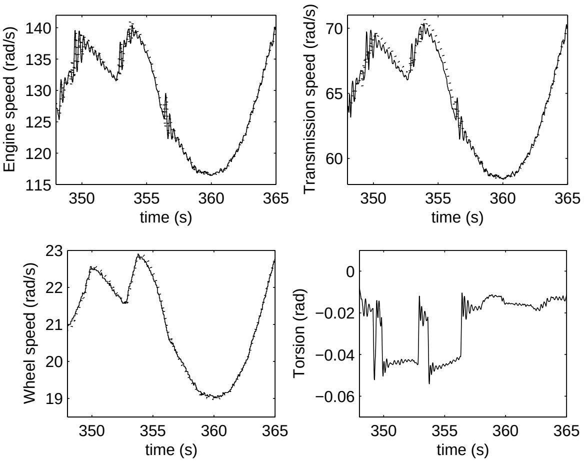

Figure 7.1. Simulated (dashed) and measured engine, transmission and wheel speed can be seen in the top figures and bottom left figure. Simulated drive shaft torsion can be seen in the bottom right picture.

shift. During some up shifts the exhaust brake is used to decrease the engine speed, and here the error is bigger than otherwise. This makes it obvious that the exhaust brake needs further modeling. The error during the other gear shifts are not as easy to derive from any specific source, but probably they are caused by the poor quality of the estimations of the engine torque and engine friction torque.

2. **Bias-Errors in the speed signals when going from acceleration to deceleration and vice versa quickly:** The cause for this fault has been identified to bad transient behavior within the estimation of the drive resistance. A better model of the drive resistance is needed to take care of this problem.

3. **The simulation is time delayed compared to the measured signal:** This is not a constant delay and is most likely caused by delays in the drive resistance, which is extensively filtered.

4. **False oscillations in the engine and transmission speed:** Some of the oscillations occurs at the wrong time and with the false frequency. Some of these problems can be deduced to the exhaust brake torque signal, which seem to be inaccurate in its timing. A linear model like the one in this thesis is not able to capture all oscillations right since some tend to change their frequency during the oscillation.

5. **Small 50 Hz oscillations in the engine and transmission speed:** As can be seen in figure 7.2, small oscillations of high frequency sometimes occur. This problem is caused by the use of different Kalman gains depending on

which new data that is available. Different magnitudes of the feedback for different Kalman filters may result in one feedback that is too strong and one feedback that is too weak, which can yield the small oscillations in figure 7.2.

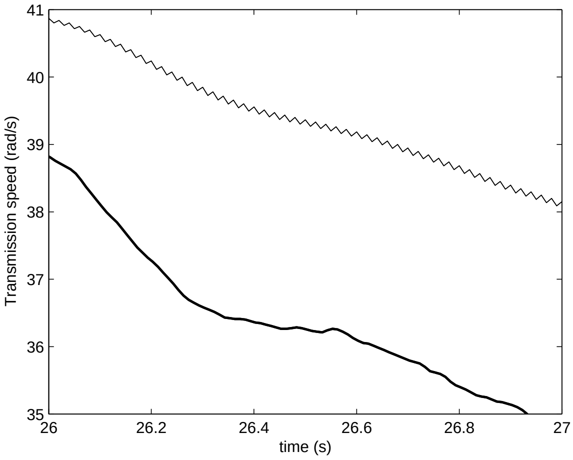

Figure 7.2. Simulated and measured (bold) transmission speed.

The problems 1-4 above are probably caused by the input signals to the model. In chapter 8, a model for the drive resistance will be added to try to improve the performance and on the same time trying to estimate the road slope. The problem 5 is dealt with in the following section.

Dealing with Problem 5

To deal with the problem caused by the use of different Kalman gains in different samples, an approach is to use the same filter in all samples and just switch depending on which gear that is engaged. However, since the engine speed and wheel speed are not updated at the same rate as the transmission speed, it is preferable only to use the difference between the simulated and measured values for these signals in the Kalman filter when a new measurement is available. Taking this into account, the feedback from the Kalman filter is smoothed out over the samples before a new measurement is available. This is done by using a smaller Kalman gain for these signals, but instead using them in every sample.

In practice this is implemented as taking the difference between the simulated and measured engine and transmission speed at their respective update frequency, and then re-sampling this difference to 100 Hz. However, the Kalman gain now has to be calculated as if the system was running at 20 Hz, the lowest of the update frequencies, to assure that the gain does not become so big it makes the system unstable. The result of this new approach is seen in figure 7.3, Comparing

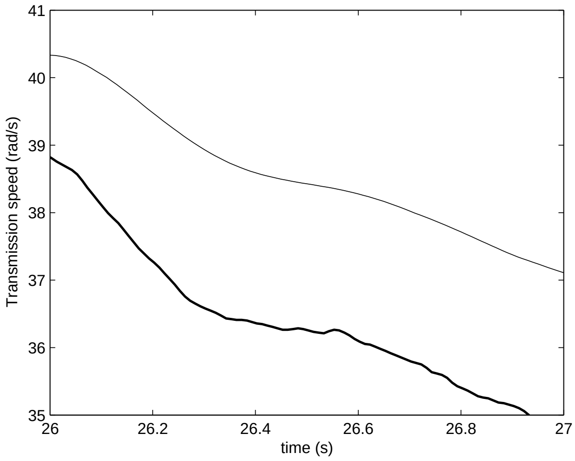

Figure 7.3. Simulated and measured (bold) transmission speed.

figure 7.3 with figure 7.2, it is obvious that the problem with the oscillations is solved.

7.5 Observer with Measurement Offset

The results of the first proposed observer shows an offset between the estimated states and the measured values. A big part of this can be explained by an inaccuracy in the measured wheel speed. In figure 7.4, the wheel and transmission speed (scaled by i_f) are shown during a short section. Here it would be correct if the signals were basically the same but with small differences due to dynamics of the drive shaft. The problem lies in the fact that the wheel speed is received as the speed of the vehicle and then transformed to rotational speed according to:

$$\omega_w = \frac{v}{r_w} \tag{7.4}$$

where v is the speed of the vehicle and r_w is the rolling radius. The sensor measuring the wheel speed is situated on the wheel and the rotational speed of the wheel is in turn transformed to vehicle speed. The rolling radius used in this transformation is however not available and therefore the wheel speed deviates from its true value. To deal with this, the wheel speed measurement is said to have a unknown dynamic offset error, which is included in the model in the manner described in section 6.5. The noise state has an empty A-matrix.

By using this approach, the observer manages to capture the dynamic offset in the wheel speed so that it is not used as a feedback in the Kalman filter. In figure 7.5, it can be seen that the estimated wheel speed now has an offset to the measured signal. Adding the offset state removes any offset error to be fed

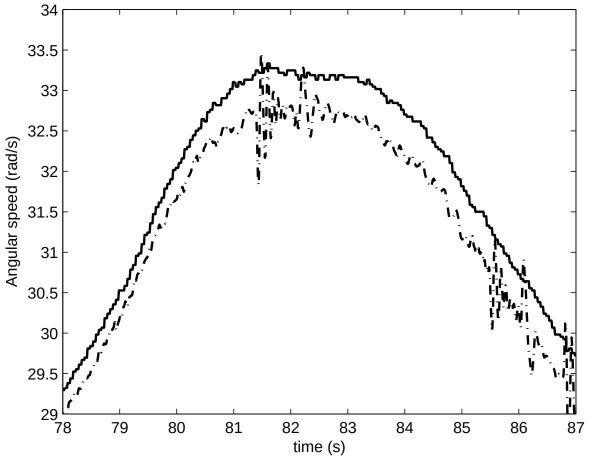

Figure 7.4. Measured wheel speed and measured and scaled transmission speed (dash-dotted).

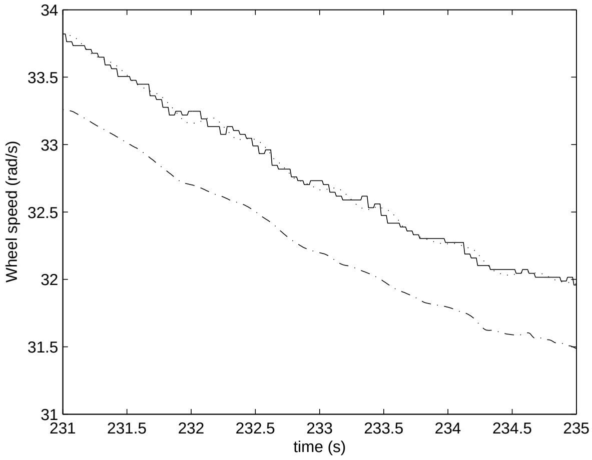

Figure 7.5. Estimated wheel speed (dash-dotted), estimated wheel speed with added offset fault (dotted) and measured wheel speed (solid).

through the Kalman filter. In figure 7.6 it is shown that this approach makes the transmission speed unbiased in comparison to the measured signal.

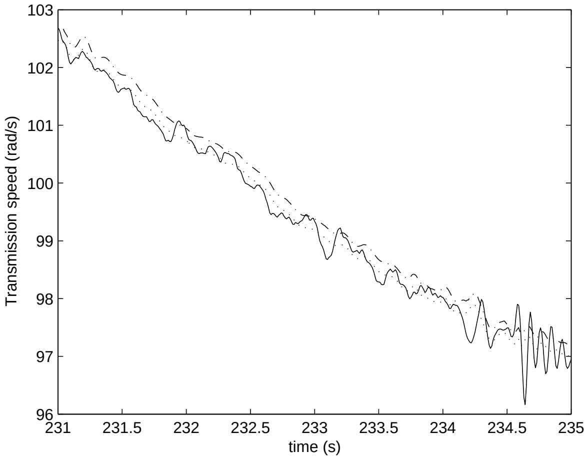

Figure 7.6. Estimated transmission speed when no offset fault is included in the model (dash-dotted), estimated transmission speed with offset fault included in the model (dotted) and measured transmission speed (solid).

7.5.1 Estimating the Rolling Radius

By introducing the wheel speed offset state, it becomes possible to estimate the rolling radius of the wheel used in first transformation of the wheel speed to vehicle speed. If v is the measured vehicle speed, e_{off} is the offset error, r_w is the given, but uncertain, rolling radius of the wheel and $\hat{r}_w$ is the real rolling radius, then in the ideal case the following relation is valid

$$\begin{aligned} \frac{v}{r_w} - e_{off} &= \frac{v}{\hat{r}_w} \Leftrightarrow \\ \hat{r}_w &= \left(\frac{1}{r_w} - \frac{e_{off}}{v}\right)^{-1} \end{aligned} \tag{7.5}$$

If the estimated radius $\hat{r}_w$ is stored in a histogram in each sample, a good estimation of the real rolling radius is to take the radius that yields the peak in the histogram. As can be seen in figure 7.7, the rolling radius adapts a value between 0.491-0.492 meter in just a few seconds. The rolling radius estimated in this way is considered a good estimation, and is used in the model where the rolling radius is needed. This makes the need for a priori knowledge of the rolling radius obsolete.

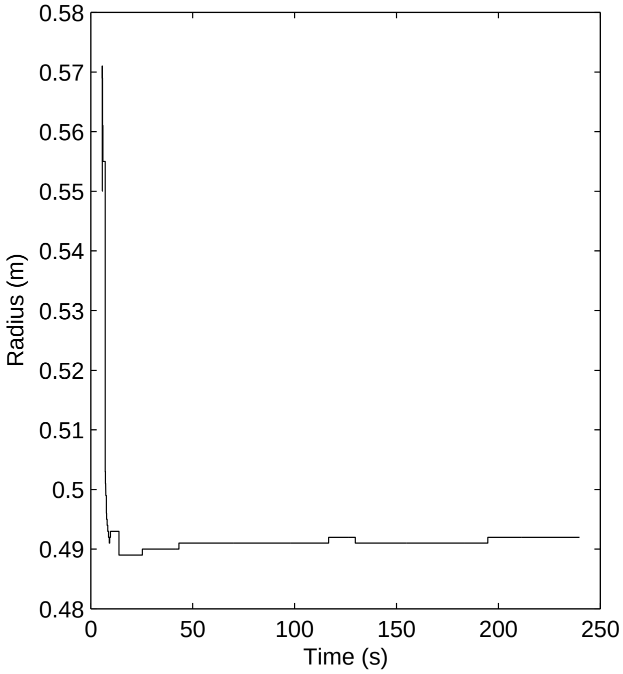

Figure 7.7. Adapted wheel radius.

7.6 Observer with Modeled Measurement Noise

Models of the measurement noise for the transmission and engine speed are added to the driveline model in hope of further smoothening of the estimates from the observer. For the wheel speed no measurement noise of significance is found, and therefore no model for the measurement noise of this signal is estimated. In this section the measurement noise is once again said to be of high frequency character. To model the measurement noise a section free from gear shifts is high pass filtered. The resulting signal is said to represent the measurement noise. Different methods can be used to model the noise. In this thesis an AR-model is chosen. The main reason for this is that it is the easiest model and the estimations of the model parameters is a linear problem. This fact also motivates its use, since it makes an on-line estimation more probable, which is an advantage in a future implementation in a truck.

7.6.1 Modeling the Noise

Modeling the noise as an AR-process means that the noise is written on the form:

$$y(t) + a_1 y(t-1) + \ldots + a_n y(t-n) \quad = \quad e(t) \tag{7.6}$$

where $y(t)$ is the measurement noise with the white noise $e(t)$ used as input to the model. The number n denotes the degree of the process. The name ”AR” comes from the fact that the signal is depending on the old values of itself, that is, the signal is **A**uto-**R**egressive. The predictor for the model in equation (7.6) is

$$\hat{y}(t|t-1) \quad = \quad -a_1 y(t-1) - \ldots - a_n y(t-n) \tag{7.7}$$

By introducing

$$\varphi(t) = \begin{pmatrix} -y(t-1) & -y(t-2) & \ldots & -y(t-n) \end{pmatrix}^T$$

$$\theta \quad = \quad (a_1 \quad a_2 \quad \ldots \quad a_n)^T$$

we can rewrite (7.6) as

$$y(t) \quad = \quad \varphi^T(t)\theta + e(t) \tag{7.8}$$

In this expression both $y(t)$ and $\varphi(t)$ are measured quantities, while $e(t)$ is white noise and θ is the vector containing the parameters to be estimated. This is a linear regressive model where θ can be estimated using the least squares method. Equation (7.6) can easily be written as a state-space model which makes it suitable for extending an already given state-space model as described in section 6.5.

To decide the order of the model, the variances of the prediction errors, $W(n)$, for different model orders are considered. The variance of the prediction error is given by

$$W(n) = V(\hat{\theta}^{(n)}) = \frac{1}{N} \sum (y(t) - \hat{y}(t))^2 \tag{7.9}$$

where n is the model order, N is the length of the signal, y is the signal to be modeled and $\hat{y}$ is the one step estimation of the signal. If the estimation data is used for this, $W(n)$ will be a strictly decreasing function and the goal is to find a model order where it stops decreasing rapidly, where there is a so called knee in the graph. In figure 7.8, $W(n)$ can be seen for the transmission speed measurement noise. The choice of model order now becomes a choice between low model complexity and finding the knee in the graph. Considering the variance of the prediction errors seen in figure 7.8, a model order of around ten would seem appropriate, but this is considered too high and a compromise of order four is chosen. The same model order is chosen for the engine speed measurement noise. These models are added to the state-space model of the driveline in the way described in section 6.5, and in the same way added to the Simulink model.

In figure 7.9 the transmission speed can be seen in the cases with and without the noise models for a short section. The estimated measurement noise for this

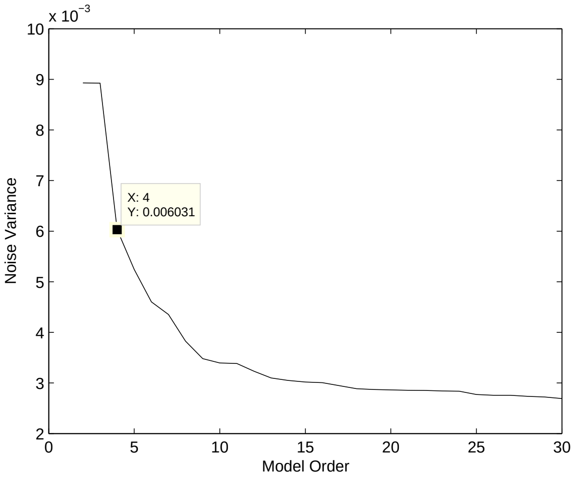

Figure 7.8. Variance of the prediction error for the estimated model of the transmission speed measurement noise.

section is seen in figure 7.10. Additionally, the measurement noise obtained when the measured signal is high-pass filtered is seen in figure 7.10. The estimated noise seem to be a good estimation if it is compared to the high-pass filtered measured signal. Nevertheless, as can be seen in figure 7.9 only small benefits are obtained by modeling the noise. The conclusion made is that no relevant advantage is given by this method, especially considering the extra complexity it would add to a real implementation of the system.

7.7 Summary

Different observers based on Kalman theory are tested and evaluated. The first approach is to use one Kalman gain for each gear and for each set of measured signals that contains new information, i.e. one set is a sample where new information in the engine and transmission speed signals is available and another is when new information is available in the wheel and transmission speed signals. This observer creates oscillating estimates of the measured signals. A second approach is tested where different Kalman gains are used for each gear not depending on the update of the speed signals. The second observer does not have the problem with the small oscillations on the estimated signals, but still has a problem with offset errors on the estimates. The offset error of the wheel speed measurement is modeled, and a another observer is created. Smooth signals with smaller bias errors on the estimations are obtained. In the last observer, a model for the measurement noise is included, but no relevant improvements are gained from the noise models. The conclusion is that the best observer is the one that includes a model of the wheel speed measurement offset error, no models for the measurement noise, and

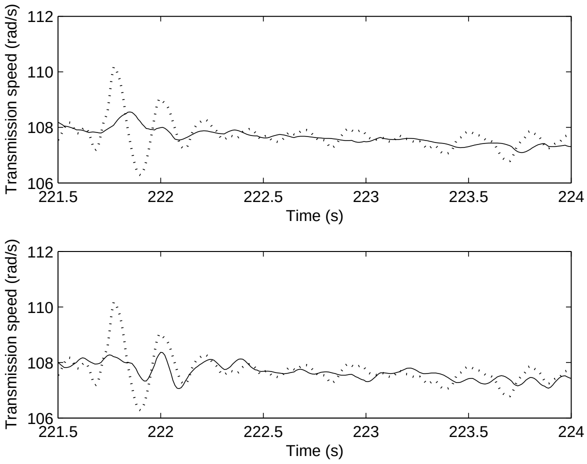

Figure 7.9. Top figure: Measured (dashed) and estimated transmission speed without the noise models. Bottom figure: Measured (dashed) and estimated transmission speed with noise model.

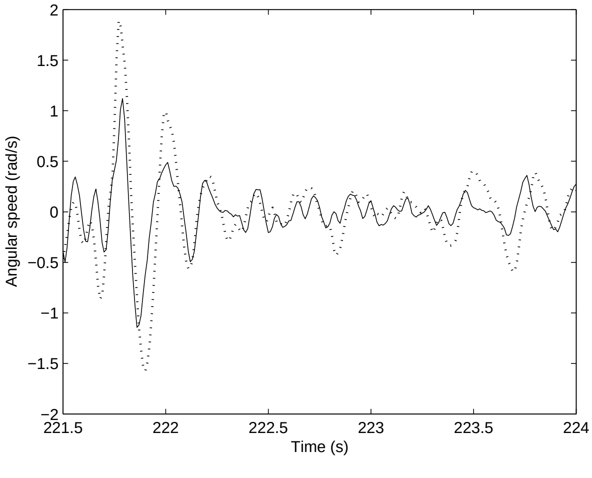

Figure 7.10. The estimated noise and the noise given by high-pass filtering the measured signal with the same filter used in the estimation (dashed).

uses one Kalman gain per gear. Problems that are still remaining mainly arise from problems with the input signals. To improve the observer, further modeling of the exhaust brake and the drive resistance is recommended. Since the purpose of this thesis is to include a model of the drive resistance, further modeling of the exhaust brake is left as future work.

Chapter 8

Modeling the Drive Resistance

In this chapter, a model of the drive resistance is introduced and a parameter estimation of the drive resistance model is performed.

The drive resistance mainly consist of three parts: the rolling resistance, the air resistance and the gravitational force arising from the slope of the road. Here, a short description of these forces is given. For more information, see for instance [11] and [12]. The forces from the disc brakes affect the driveline model in the same manner as the drive resistance. This fact will be dealt with later, and to begin with no brakes are assumed.

8.1 The Rolling Resistance

When a wheel is rolling, energy losses occur due to deflection of the tire. A standardized process for measuring the rolling resistance of truck and bus tires is described in ISO9948. The longitudinal force acting on a truck arising from the rolling resistance is in this thesis calculated as

$$F_{roll} \quad = \quad mg\cos\alpha\left(C_{r,iso} + C_a(v^2 - v_{iso}^2) + C_b(v - v_{iso})\right) \qquad (8.1)$$

which is a formula proposed by the tire manufacturer Michelin. The parameter $C_{r,iso}$ is given by the measurements according to ISO9948, and $v_{iso} = 80$ km/h, also according to ISO9948. C_a and C_b are constants specific for the tire. The road incline is expressed by α. The constant g is the gravitational acceleration of the earth. From previous tests at Scania, estimations of the parameters in equation (8.1) are given. These are later in this section referred to as ”Scania parameters”.

8.2 The Air Resistance

The longitudinal air resistance force acting on a truck can according to [13] be expressed by

$$F_{air} = \frac{\rho}{2} C_{drag} A_{front} (v + v_{wind})^2 \tag{8.2}$$

where ρ is the density of the air, A_{front} is the projected front area of the truck and C_{drag} is the coefficient of aerodynamic resistance. The speed of the vehicle is expressed by v, and the speed of the wind is expressed by v_{wind}. In this work the wind speed is neglected ($v_{wind} = 0$). Estimations of the parameters given in equation (8.2) are known for Scania test trucks.

8.3 Road Incline

The last part of the drive resistance is the force that arise when driving the truck in a slope. Assuming that the incline of the road is α, the longitudinal force acting on the truck is given by

$$F_{incline} = mg \sin\alpha \tag{8.3}$$

8.4 The Drive Resistance Model

Letting F_{dr} denote the driving resistance and summing up the forces given in section 8.1, 8.2 and 8.3 yields

$$\begin{aligned} F_{dr} &= F_{roll} + F_{air} + F_{incline} \\ &= mg\cos\alpha(C_{r,iso} + C_a(v^2 - v_{iso}^2) + C_b(v - v_{iso})) \\ &\quad + \frac{\rho}{2} C_{drag} A_{front} v^2 + mg \sin\alpha \end{aligned} \tag{8.4}$$

By assuming that α is small, approximations of the trigonometrical terms are made. If $\sin(\alpha) \approx \alpha$ and $\cos(\alpha) \approx 1$, equation (8.4) can be simplified to

$$\begin{aligned} F_{dr} &= F_{roll} + F_{air} + F_{incline} \\ &= mg(C_{r,iso} + C_a(\omega_w^2 r_w^2 - v_{iso}^2) + C_b(\omega_w r_w - v_{iso})) \\ &\quad + \frac{\rho}{2} C_{drag} A_{front} \omega_w^2 r_w^2 + mg\alpha \end{aligned} \tag{8.5}$$

since $v = \omega_w r_w$ if no slip is assumed. Further, by defining

$$A = mg(C_{r,iso} - C_a v_{iso}^2 - C_b v_{iso}) \tag{8.6}$$

$$B = mgC_b r_w \tag{8.7}$$

$$C = mgC_a r_w^2 + \frac{\rho}{2} C_{drag} A_{front} r_w^2 \tag{8.8}$$

equation (8.4) can be rewritten as

$$F_{dr} = A + B\omega_w + C\omega_w^2 + mg\alpha \tag{8.9}$$

8.5 Identification of the Drive Resistance Parameters

An identification of the parameters A, B and C in equation (8.6)-(8.8) is performed. Assuming that the road incline α is zero and putting the gearbox into neutral state yields

$$m\dot{v} = -F_{dr} = -A - B\omega - C\omega^2 \tag{8.10}$$

By measuring the vehicle speed when the gearbox is put into neutral state and numerically differentiating it with the Euler forward method, it is possible to use the least squares method to estimate values for A, B and C. The losses from internal friction are never avoided and therefore these are unavoidably included in the parameters obtained from the identification test in this chapter. This can be seen as a further reason to put the internal friction parameters b_i in the driveline model to zero.

Validation of the Parameters

Since it is hard to find a road section with an exactly flat road, a relatively flat road is driven in both directions and data sets from both these runs are used for the estimation. This procedure is thought to even out the faults acquired from the small slope of the road. Two further data sets are used to validate the estimated parameters, and the results of this can be seen in figure 8.1. The validation is done by using the measured wheel speed in (8.10) and integrating

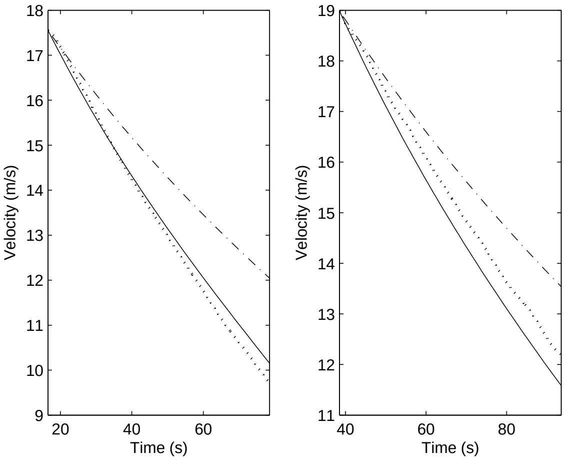

Figure 8.1. Measured velocity (dotted), estimated velocity from identified parameters (solid) and estimated velocity from previously identified parameters at Scania (dash-dotted).

the calculated acceleration. Also included in the picture is the estimated velocity when using parameters given from a previous experiment made at Scania together with parameters acquired from the tire manufacturer.

The estimated velocity from the identified parameters show relatively good agreement. In one direction the estimated velocity lies above the measurement and in the other direction it lies under the measurement. Since the road is not exactly flat this is to be expected. The reason for the bad behavior using the ”Scania parameters” is probably derived from two facts. First, the parameters are not estimated for this specific truck. Second, the rolling resistance parameters are given under the conditions in ISO9948, which means that the tires are driven until a constant temperature in the wheel is achieved. In the test runs in this section, the tires have a too low temperature compared to the values when the measurements are performed according to ISO9948. A higher tire temperature gives a lower rolling resistance, see [12], which could explain some of the differences.

8.6 Implementation of the Drive Resistance

The drive resistance is implemented in the observer according to equation (8.5). However, since the road slope is unknown it has to be estimated. This is done by making the road slope a new state which is considered to be constant but disturbed by white noise. The equation for the road slope state is given as

$$\dot{\alpha} = \dot{x}_5 = v_{1,\alpha} \tag{8.11}$$

where $v_{1,\alpha}$ is system noise. This state is only driven by the Kalman filter implemented in chapter 9.

8.7 Summary

A drive resistance model is described consisting of three parts. The drive resistance model in this chapter includes a Michelin quadratic rolling resistance model described in ISO9948, a quadratic air resistance model and the drive resistance that arise from the road slope.

Chapter 9

Observer Design with Non-Linear Drive Resistance Model

In chapter 8 a non-linear drive resistance model is developed. In this chapter a new Kalman filter making it possible to estimate the road slope is introduced.

9.1 Linearizing the Drive Resistance

With the inclusion of the drive resistance model given in the previous chapter, the driveline model becomes non-linear. The Kalman filter calculated in the previous chapters requires a linear model, which makes a new approach necessary. To deal with this, a method using linearization of the model is used.

The drive resistance is the only part in the extended driveline model that includes non-linear terms. Therefore it is sufficient to linearize the drive resistance. If ω_w^{lin} and α^{lin} are the points to linearize about, the linearized drive resistance becomes

$$\begin{aligned} F_{dr}^{lin} &= \frac{\partial F_{dr}}{\partial \omega_w}\omega_w \Big|_{\omega_w^{lin}} \omega_w + \frac{\partial F_{dr}}{\partial \alpha}\alpha \Big|_{\alpha^{lin}} \alpha + A \\ &= \left(B + 2C\omega_w^{lin}\right)\omega_w + mg\alpha + A \qquad (9.1) \end{aligned}$$

Note that linearizing with respect to α makes no difference in comparison with the non-linearized drive resistance, since it is already linear in α. That is, there is no need to choose a point α^{lin} to linearize about.

9.2 Kalman Filter Design Methods for the Non-Linear System

In this work two design methods for the Kalman filter of the non-linear system are considered, extended Kalman filter and a variant of the constant gain extended Kalman filter. The extended Kalman filter linearizes the model on-line and calculates a new Kalman gain every sample from the linearized model. The constant gain extended Kalman filter calculates Kalman gains for certain linearization points off-line, and the Kalman filter then switches between these linearizations depending on which linearization point is closest to the current working point.

9.3 Choosing Linearization Points

Linearizing the model means introducing a further model error, that increases with the distance between the working point and the linearization point. The extended Kalman filter therefore calculates a linearization of the model in the current working point and then calculates the Kalman gain from this linearization. This means that a large number of calculations are necessary every sample, and therefore this method is not commonly used in real time implementations. For the driveline model together with the extensions given by equations (8.11) and (9.1) it turns out that no advantage is gained from linearizing in every working point. Therefore an extended Kalman filter is not considered necessary, and instead a variant of the constant gain extended Kalman filter is used. One linearization velocity is chosen for every gear and this linearization is used to calculate the Kalman gain for that gear. The linearization points are chosen so that the truck runs at 90 km/h on the highest gear, which corresponds to an engine speed of 1215 rpm. This can in turn be recalculated to a wheel speed for every gear as

$$\omega_w^{lin} = \frac{\omega_e^{desired}}{i_t i_f i_{hub}} \tag{9.2}$$

where $w_e^{desired}$ is the desired engine speed, 1215 rpm.

9.4 Estimating the Road Slope

With the use of the Kalman design method introduced above, an estimation of the road slope is produced. The design parameters of the Kalman filter are as before the intensities of the system and measurement noise Q and R, where Q now also includes an element for the intensity of the road slope state system noise. This element is a choice between speed and noise sensitivity of the road slope estimation. The results from two estimations with different Kalman gains can be seen in figure 9.1. The truck is driven downhill with 8%, 4% and 6% slope. As can be seen the estimations are fairly accurate, and as expected the noisier estimation has a faster transient behaviour. To try and capture a faster transient behavior without capturing too much noise in the road slope estimations, a second approach

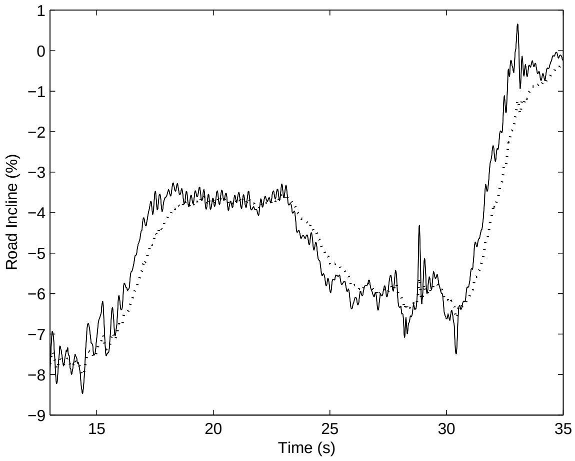

Figure 9.1. Road slope estimations with two different Kalman gains.

for estimating the road slope is tested. This involves a state for the derivative of the road slope. The road slope is now described by

$$\dot{\alpha} = \dot{x}_5 = x_6 \tag{9.3}$$

$$\ddot{\alpha} = \dot{x}_6 = v_{1,\alpha} \tag{9.4}$$

instead of equation (8.11), meaning that the second derivative of the road slope instead of the first derivative is purely white noise. A result from this approach in comparison with the faster of the two estimations in figure 9.1 can be seen in figure 9.2. As can be seen, the new approach in equation (9.3) and (9.4) gives a slightly less noisy signal with the same transient behavior, but the signal is still noisy and further improvement is desirable.

9.4.1 Spike Reduction in the Road Slope Estimation

At some points the road slope estimation show big spikes. Examples of these spikes can be seen in figure 9.3. The spikes are caused by oscillations in the driveline which the model is unable to capture. Three origins for these spikes are identified:

1. **Zero torque crossing:** When the torque in the driveline passes zero, oscillations occur which are caused by a backlash in the gearbox and clutch. This phenomena is not included in the model.
2. **Engagement of exhaust brake torque:** The exhaust brake gives a very sudden change in torque, causing oscillations. The signal for this torque is however very inaccurate, making the model inaccurate in predicting these oscillations.

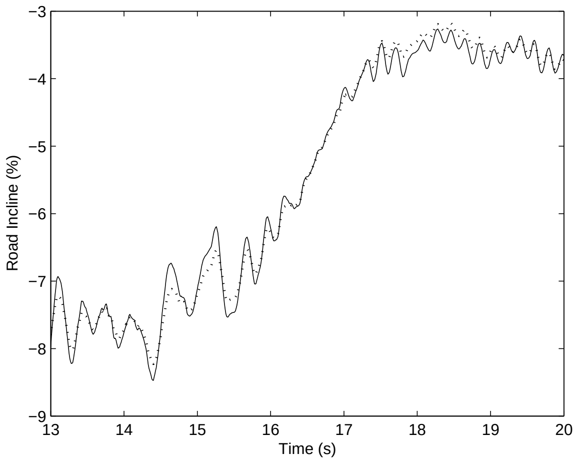

Figure 9.2. Road slope estimation when saying that its acceleration is zero (dashed) and when saying its speed is zero (solid).

3. **Gear engagement:** When a new gear is engaged this causes rattles in the gearbox, which in turn causes oscillations in the driveline. These oscillations are also not part of the model.

To try and reduce the effects on the road slope estimation caused by these model inaccuracies, the gain from the Kalman filter is decreased during a period of 0.5 seconds after the occurrence of one of the factors mentioned above. The time 0.5 seconds is chosen as the approximative time it takes for the worst oscillations to vanish. The result from this approach is illustrated in figure 9.3. As intended most big spikes are removed with this method. The big disadvantage is however, that if many of these oscillations occur near each other in time, the feedback to the road slope state will be low for a long time and therefore giving the road slope estimation a bad transient behavior during these periods.

9.4.2 Comparison between Drive Resistance Parameters

In section 8.5 two sets of parameters for the drive resistance are validated. In figure 9.4 road incline estimations made with the different sets of parameters can be seen. There is no relevant difference in the dynamics of the estimations, but it is rather a pure offset difference. The difference is relatively small, and since only approximately ”correct” values for the road slope are known it is hard to assess which of the estimations is better. However, the parameters previously identified seem to give better values while driving on a supposedly flat road. More and longer tests are required to further investigate if the parameters acquired from tire manufacturers and physical data are accurate enough. This is preferable if a model is to be implemented in many different trucks, since it is not possible to perform thorough identification tests for every truck off-line.

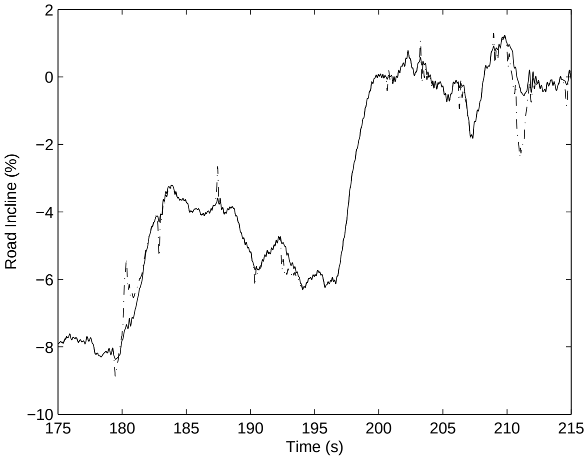

Figure 9.3. Road incline estimation with (solid) and without (dash-dotted) the method to reduce spikes.

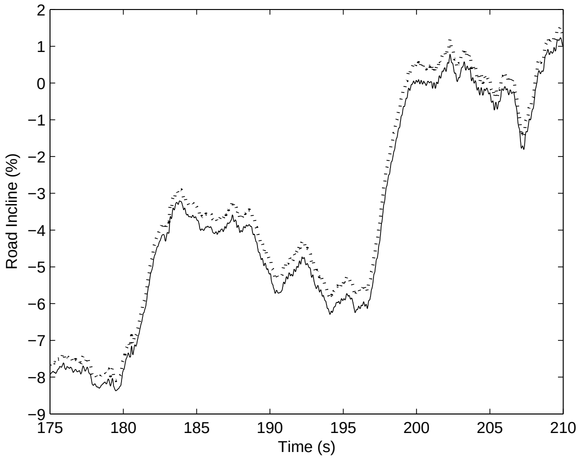

Figure 9.4. Road incline estimations made with different parameters for the drive resistance. Dashed line represents parameters acquired from tire manufacturer and physical specifications, solid line represents parameters identified in previous chapter.

9.5 The Disc Brakes

The disc brakes are normally not seen as a part of the drive resistance, but the torque they cause on the wheels enters the driveline model in exactly the same way as the drive resistance. To be able to estimate the road slope when the brakes are engaged in the way proposed in this chapter, it is necessary to have a measurement or estimation of the torque caused by the brakes. The only information available to the Opticruise control system concerning the brakes, is how much the brake pedal is depressed. A static model of the relationship between the brake pedal, speed and brake torque has been tested, but the results have not been satisfactory. The reasons for this are that the pressure from the brakes is not only dependent on the brake pedal position, but for instance also on the temperature of the brakes and the wearing of the brakes. Additionally, the resulting brake drum pressure in the brakes is controlled by a controller which makes it even more difficult to make an estimation of the brake torque from knowledge about the brake pedal position. Therefore it is probably necessary to have a measurement of the brake drum pressure to get a satisfactory static model of the brake torque. An investigation concerning this relationship can be seen in [14]. This approach is not pursued any further in this thesis since no signal measurement of the brake pressure has been possible to produce to the Opticruise system. Instead the use of an accelerometer for the road incline estimation will be investigated further. The accelerometer makes the road slope estimation possible also when the disc brakes are engaged, see chapter 11.

9.6 Summary

The driveline model is extended with the non-linear drive resistance model described in chapter 8, and a new Kalman filter is calculated. To design the new observer, a variant of the constant gain extended Kalman filter is used. To use this method the model is first linearized, and the road slope is introduced as a state purely driven by the Kalman filter. It is further shown that a less noisy road slope estimation is obtained if the road slope state is driven by a state describing the derivative of the road slope which in turn is driven by the Kalman filter. Spikes in the road slope estimation are deduced to zero torque crossing, the use of the exhaust brake and the engagement of a new gear. A weaker Kalman gain is used in these situations to reduce the spikes.

Chapter 10

Sensor and Parameter Analysis

In this chapter, the observer in chapter 9 is further evaluated. Investigations of the effect from removing different sensors are made, as well as examinations of the effects from changes in parameter values.

10.1 Sensor signals

It is interesting from a technical perspective as well as from a financial view to evaluate the need for different sensors. Is it for instance possible to replace the Opticruise sensor by the tachograph that according to the law is required in most trucks? A description of the method for the evaluation and the results from the evaluation of different sensor configurations follow in the following sections.

10.1.1 Method

Sensors are removed and new Kalman gains are calculated for different sensor combinations using the observer in chapter 9. The measure used for comparing the different observers is the expectation value of the relative deviation and the relative maximum deviation between the estimated signals and non-causal low pass filtered measured signals. Comparison with non-causal low pass filtered signals are made since the goal is to get smooth non-time-delayed signals. The filtering is performed in a non-causal manner using the Matlab command `filtfilt`, which means that no time-delays are introduced.

Measuring only some of the signals can yield an unobservable system. To simplify the comparison, the offset state for the wheel speed sensor is removed for the measurement setups not containing all three signals. Doing this makes the system observable even if not all the signals are measured. Still, the system is not observable in the disengaged mode if only one signal is measured. To trim the relationship between the measurement and process noises, i.e. Q and R matrices for the different cases, the observer is evaluated for a range of different quotients between these and the quotient that minimizes the expectation error of the transmission speed is used.

Modeling the offset error improves the observer when the rolling radius is uncertain. For these experiments the rolling radius is set to the right value obtained from previous estimations, which makes the effect from the offset state small. It has to be kept in mind that removing the rolling radius state may reduce the accuracy of the model even though it is not visible in the experiments in this chapter.

10.1.2 Comparison Between the Transmission Speed Sensors

Since there are two sensors measuring the speed of the gearbox's output shaft, it is interesting to investigate how much difference it makes using the tachograph speed as a measured signal in the Kalman filter instead of the signal from the Opticruise sensor.

A comparison of the driveline observer using the two different signals for the transmission speed can be seen in table 10.1. The comparison shows that there are only a small differences between the shaft speeds in the two cases. The results indicates that it may be possible to remove the Opticruise sensor and to use the tachograph instead. From a financial perspective this is a promising result. The increase in the relative maximum deviation when the tachograph is used can be deduced to the tough filtering of the tachograph speed. In figure 10.1 the difference between using the two measured signals can be seen for the transmission speed estimates. The only difference is a small time delay of approximately 0.03 seconds. This is of course not desirable, but the effect of this time delay to the systems is not explored in this thesis.

	Engine Speed	
	Rel. Mean Deviation	Rel. Max Deviation
Opticruise sensor	0.3%	4.5%
Tachograph	0.3%	4.5%
	Transmission Speed	
	Rel. Mean Deviation	Rel. Max Deviation
Opticruise sensor	0.2%	2.2%
Tachograph	0.3%	2.9%
	Wheel Speed	
	Rel. Mean Deviation	Rel. Max Deviation
Opticruise sensor	0.1%	1.3%
Tachograph	0.1%	1.3%

Table 10.1. Relative mean and relative maximum deviation of the engine, transmission and wheel speed in comparison with a low pass filtered signal.

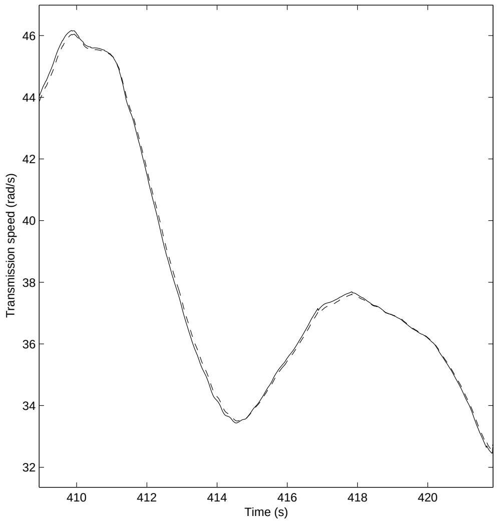

Figure 10.1. Transmission speed estimation using the tachograph sensor (dashed) and the Opticruise sensor (solid).

10.1.3 Different Sensor Configurations

Sensor configurations where only one ore two signals are measured are also tested. Measuring only one or two of the different speed signals makes it possible to use nine different sensor configurations if not both the Opticruise sensor and the tachograph are used in the same configuration. As can be seen in table 10.2, there are no huge differences in the mean deviation of different speeds for the different observable configurations. The configurations which yield unobservable states make a relevant increase both in the mean deviation and in the maximum deviation. This is expected since there is no knowledge about the unobservable states.

10.1.4 Conclusions

In general, good results are achieved for the sensor configurations that make the entire system observable. If all three speeds are measured, there are only small differences between using the Opticruise sensor and the tachograph. With two measurements, the estimations are still good, but only if the system is observable. For all configurations that makes the system unobservable, the unobservable states show major increases in the relative maximum deviation, and relevant changes in the mean of the relative deviation. All together the tests show that the observer show good performance even if a loss of one of the sensors occur.

In the experiments in this chapter, the rolling radius of the wheel is accurately known. In other situations, this might not be the case. In these cases, the observers that do not model the wheel speed offset will show larger deviations in the observed states. Therefore, it is desirable to have a sensor set that makes it possible also to model the wheel speed offset, meaning a set of sensors that measure engine, transmission and wheel speed.

10.2 Parameter Sensitivity

It is interesting to check the sensitivity of the observer with respect to the parameters. If the observer is able to create good and smooth estimates of the desired signals even though the parameters are changed, the observer is considered to be robust with respect to changes in the parameters. This is a desired property since the owner of a truck can switch to new drive shafts and tires with other physical parameters than those delivered with the truck without modifying the software.

10.2.1 Method

In section 4.3 the sensitivity of the driveline model with respect to the parameters is examined. It is shown that the most sensitive parameters are the mass, wheel radius, drive shaft stiffness and damping. The observer is therefore examined regarding variations in these parameters in the same manner as for the stand alone model. The observer is not expected to be more sensitive to parameter changes than the driveline model examined in chapter 4.3, and changes in the parameters to which the model was insensitive before are therefore not examined here.

Variations in the Mass

Changing the mass of the truck within a reasonable range (10-60 tons) has no effect on the speed signals and shaft torsion. The only affected output of the observer is the road slope estimation. This is mainly caused by the fact that the part of the drive resistance originating from the gravitational force is changed. This implies that if the road slope is to be estimated accurately, it is important to have a good estimation of the mass. A method for estimating the mass of the vehicle is described in section 11.8.

Variations in the Rolling Radius

The estimation of the rolling radius developed in section 7.5.1 is not used now. Instead, the rolling radius is held constant at different values. The effect of changes in this parameter is basically the same as for the mass, namely that just the road slope estimation is affected. This is caused by the transformation of the drive resistance forces to drive resistance torques using the rolling radius.

Variations in the Shaft Stiffness

Changes in the stiffness of the shaft causes changes in the frequencies of the oscillations in the driveline in the same manner as can be seen in section 4.3.2. It also affects the torsion in a way that a 30% increase in the stiffness causes a 30% scaling of the torsion. If the shaft stiffness is set too high, numerical problems can make the observer diverge.

Variations in the Shaft Damping

The damping coefficient has the same affect on the observer as on the model without the feedback, which can be seen in section 4.3.2. If the damping coefficient is set to low, numerical problems can make the observer diverge.

10.2.2 Conclusions

The observer is robust against changes in the mass and rolling radius if the road slope estimation is not considered. However, to get a good estimation of the road slope, correct values of these parameters are necessary. The adaption of the rolling radius is therefore necessary, and it will only affect the road slope estimation during its settling time. An estimation of the mass of the vehicle is developed in section 11.8, and this estimation will only have an effect on the road slope estimation during its settling time. The stiffness and damping coefficient of the shaft have their main affect on the oscillations and the torsion. Since no measurement of the torsion is available, a validation of the torsion is hard to perform. Therefore, the torsion is not considered more thoroughly.

	Engine Speed	
Measured Speed Signals	Rel. Mean Deviation	Rel. Max Deviation
Engine, Wheel	0.3%	4.5%
Engine, Transmission (Opticruise)	0.3%	4.5%
Engine, Transmission (Tachograph)	0.3%	4.5%
Transmission (Opticruise), Wheel	2.0%	17.2%
Transmission (Tachograph), Wheel	2.0%	17.2%
Engine	0.3%	4.5%
Transmission (Opticruise)	1.9%	17.1%
Transmission (Tachograph)	1.9%	17.1%
Wheel	2.0%	17.6%

	Transmission Speed	
Measured Speed Signals	Rel. Mean Deviation	Rel. Max Deviation
Engine, Wheel	0.4%	3.8%
Engine, Transmission (Opticruise)	0.2%	2.4%
Engine, Transmission (Tachograph)	0.3%	2.8%
Transmission (Opticruise), Wheel	0.3%	3.1%
Transmission (Tachograph), Wheel	0.3%	3.3%
Engine	0.8%	9.7%
Transmission (Opticruise)	0.2%	2.7%
Transmission (Tachograph)	0.3%	2.9%
Wheel	0.4%	3.9%

	Wheel Speed	
Measured Speed Signals	Rel. Mean Deviation	Rel. Max Deviation
Engine, Wheel	0.1%	1.6%
Engine, Transmission (Opticruise)	0.3%	1.8%
Engine, Transmission (Tachograph)	0.2%	1.4%
Transmission (Opticruise), Wheel	0.1%	1.1%
Transmission (Tachograph), Wheel	0.1%	1.1%
Engine	0.8%	9.2%
Transmission (Opticruise)	0.3%	2.0%
Transmission (Tachograph)	0.2%	2.9%
Wheel	0.1%	1.7%

Table 10.2. Relative mean and relative maximum deviation of the engine, transmission and wheel speed in comparison with a low pass filtered signal for different measured signals.

Chapter 11

Contributions from an Accelerometer

A one-dimensional accelerometer is mounted in the truck. The sensor and its applications are discussed in this chapter. With the help from the accelerometer, a road slope estimation that works during engagement of the disc brakes is developed. Additionally, a mass estimation based on the accelerometer signal is produced.

11.1 The Sensor

The acceleration measurement is performed using a capacitive sensor made of silicon and glass. Initially the sensor is placed in two different positions for comparison. The first position is in the cabin under the glove compartment, and the second position is behind the cabin on the frame of the truck. Figure 11.1 shows that the disturbances on the sensor placed on the frame has a higher frequency and smaller amplitude than the sensor placed in the cabin. The disturbances on the sensor on the frame is believed to mainly originate from vibrations caused by the engine. The sensor in the cabin is also disturbed by vibrations caused by the engine, which are transferred through the suspension system of the cabin. Additionally, factors as wind and sudden changes in acceleration will cause the cabin to move. During braking this phenomena is called tip-in, and significant changes can be seen in the sensor values. Since a higher frequency and smaller amplitude in the disturbances is considered easier to distinguish from the desired signal, the sensor location on the frame is used for further processing.

The accelerometer is mounted parallel to the ground and measures the sum of the truck's acceleration and the gravitational component parallel to the ground, that is

$$a_{sensor} = \dot{v} + g\sin(\alpha) \tag{11.1}$$

where a_{sensor} is the sensor value, v is the velocity of the truck and α is the

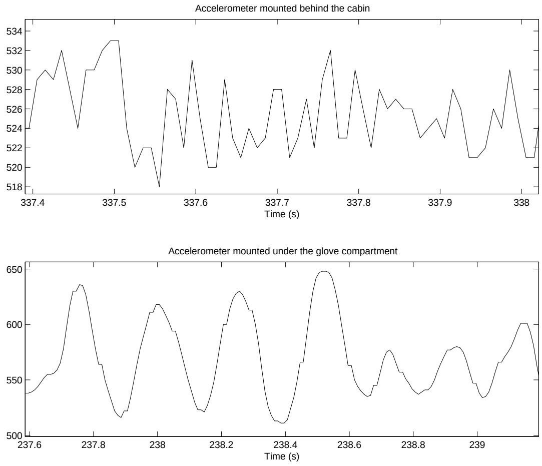

Figure 11.1. Top figure: Raw accelerometer signal when the sensor is placed on the frame behind the cabin. Bottom figure: Raw accelerometer signal when the sensor is placed under the glove compartment.

road inclination. One problem with the sensor is its sensitivity to accelerations perpendicular to the direction of measurement, and this will be discussed in section 11.5 below.

11.2 Calibration

In this thesis, the calibration of the accelerometer is manually performed by placing the truck two times on the same spot but in opposite directions. Since the accelerometer is supposed to give the same road incline (with the exception of the sign) in the two different directions, it is possible to calculate the offset on the sensor.

If the sensor is to be used in production, an automatic offset calibration has to be performed, since the load of the truck and the setting of the air suspension may affect the inclination of the sensor itself. A possible way to make a calibration of the accelerometer is to use the two different estimations of the road slope created by the driveline observer and the road incline filter.

11.3 Road Incline Estimation

A model for road slope estimation using an accelerometer is proposed in [15]. In the article, the model

$$\begin{pmatrix} \dot{v} \\ \dot{\alpha} \end{pmatrix} = \begin{pmatrix} 0 & -g \\ 0 & -\omega_c \end{pmatrix} \begin{pmatrix} v \\ \alpha \end{pmatrix} + \begin{pmatrix} a_{sensor} \\ 0 \end{pmatrix} + \begin{pmatrix} w_1 \\ w_2 \end{pmatrix} \tag{11.2}$$

is stated for estimation of the road incline. Here, w_1 and w_2 are white noise and ω_c is the cut-off frequency of the road slope. In this work, the model described by equation 11.2 is simplified, and the road incline is modeled with a zero A-matrix. The system in this work is now given by

$$\begin{pmatrix} \dot{v} \\ \dot{\alpha} \end{pmatrix} = \begin{pmatrix} 0 & -g \\ 0 & 0 \end{pmatrix} \begin{pmatrix} v \\ \alpha \end{pmatrix} + \begin{pmatrix} a_{sensor} \\ 0 \end{pmatrix} + \begin{pmatrix} w_1 \\ w_2 \end{pmatrix} \tag{11.3}$$

The first row of equation (11.3) is simply a restatement of equation (11.1), and the zeros in the row for the road incline state means that the road incline estimation is purely driven by white noise. A Kalman filter for model 11.3 is implemented using the vehicle speed as input to the feedback, which yields the filter

$$\begin{pmatrix} \dot{\hat{v}} \\ \dot{\hat{\alpha}} \end{pmatrix} = \begin{pmatrix} 0 & -g \\ 0 & 0 \end{pmatrix} \begin{pmatrix} \hat{v} \\ \hat{\alpha} \end{pmatrix} + \begin{pmatrix} a_{sensor} \\ 0 \end{pmatrix} + K \begin{pmatrix} v - \hat{v} \end{pmatrix} \tag{11.4}$$

K is calculated as described in chapter 6, where Q and R are the design parameters of the filter.

11.4 Evaluation of the Road Slope Filter

The filter is simulated, and the result can be seen in figure 11.2. The estimated road slope is a good approximation of the real slope. The dip at 405-408 seconds can be explained by the fact that the truck is turning, and hereby generating an acceleration in the perpendicular direction compared to the direction of the accelerometer. Hence, the filter is good in non-turning driving situations, while during cornering other methods have to be used to estimate the road slope.

Another problem occurs when a big braking torque is applied. A plot of the estimated road incline during hard braking can be seen in figure 11.3. Since the truck used in the experiments is heavy in the front, a probable explanation to the dip is that the truck is dipping itself. The problem does not occur during braking with a more ”normal” torque and is not considered to be of big importance.

11.5 Compensating for Perpendicular Acceleration

As shown in figure 11.2 the road incline observer does not manage to make a correct estimation of the road slope while cornering because of the centripetal acceleration this causes. Since the accelerometer is disturbed by perpendicular acceleration, it is wishful to compensate for this disturbance. A proposed linear relation between a calculated centripetal acceleration and the disturbance on the sensor has been tested without satisfying results. Further work in this area is needed if any good results based on the accelerometer while cornering are to be extracted.

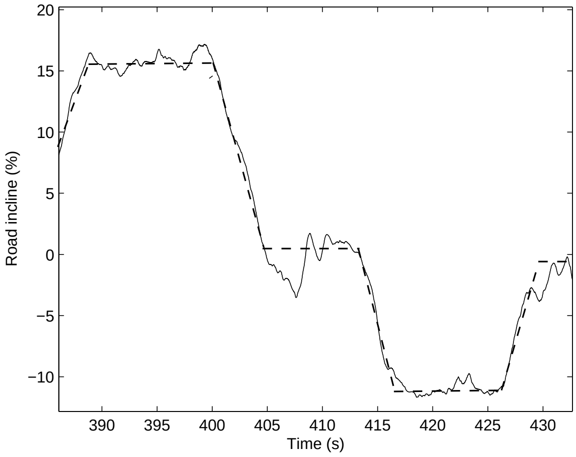

Figure 11.2. Road incline estimation. Solid line: Estimated road incline using the observer 11.4. Dashed line: Approximate road incline according to road map.

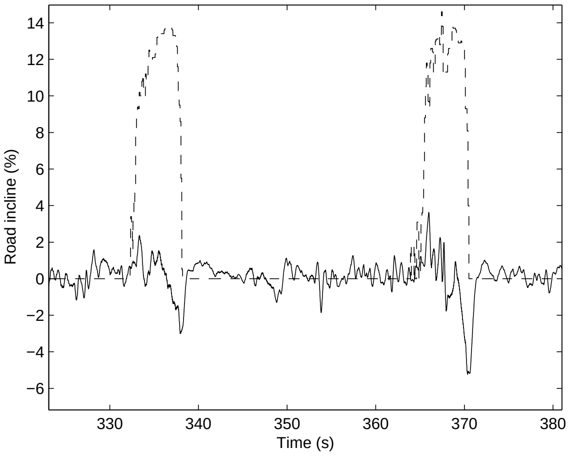

Figure 11.3. Road incline during hard braking. Solid line: Road incline. Dashed line: Indicated brake pedal position. The numerical values of the latter are scaled to fit in the plot.

11.6 Combining the Accelerometer with the Observer

Different methods can be used to include the road slope estimated in the filter in (11.4) in the driveline observer. Two different approaches are considered:

1. Use the road incline in (11.4) as input to the drive line model.
2. Use the road incline in (11.4) as a measured signal in the feedback in the driveline observer.

The estimation of the road slope produced by the observer in chapter 9 and the filter in equation (11.4) have different benefits. Using the observer from chapter 9 for estimating the road slope is only possible in situations when the truck is not using the disc brakes. On the other hand, (11.4) can only be used when the vehicle is not making hard turns since the sensor is sensitive to perpendicular acceleration. The best overall results are achieved when method 2 is used but different Kalman filters are calculated depending on the situations, meaning extremely hard reliance on the measured road slope signal during braking and practically no reliance on the measured road slope signal during cornering. This approach is used in the simulations and validation described in chapter 12.

11.7 Estimation of Brake Torque

Using the driveline observer and the road incline filter described in this chapter, it should be possible to make an estimation of the disc brake torque during braking. During braking without a state for the disc brake torque, the road incline estimated in the driveline observer tends to increase. The belief is that this increase corresponds to the brake torque. The brake force is therefore introduced as a new state just driven by noise, and a hard reliance is put on the signal from the road incline filter which is supposed to make it possible to make an estimation of the brake force. No successful trials have been performed, but it is nevertheless believed that it is possible to create an estimation of the disc brake torque by using a hard feedback on the signal from the road incline filter. To do this, further trials have to be performed.

11.8 Mass Estimation

The mass of a truck can vary significantly depending on the amount of load. This makes it vital to have an adaptive estimation of this parameter. Making the mass a state in the model of the driveline will make the model even more non-linear, which is not wishful. Considering the small influence the mass has on the outputs of the observer (except on the road slope) a fast separate estimation of the mass is made. Using this mass as an input to the driveline model will only affect the road slope estimation from the driveline observer during a short period after a reload.

The adaptive filter is based on Newton's second law, which yields

$$F_{resulting} \quad = \quad m_{tot}\dot{v} \tag{11.5}$$

where $F_{resulting}$ is the sum of all forces acting on the truck, $\dot{v}$ is the acceleration and m_{tot} is the total mass to be accelerated. The resulting force is the sum of the driving force and the driving resistance, and can be extracted from the Simulink model of the driveline observer. The equation for the wheel yields

$$J_w\dot{\omega}_w = T_w - T_{resist} \tag{11.6}$$

where T_w is the torque on the wheel and T_{resist} is calculated from

$$m\dot{v} = F_{resist} - F_{dr} \tag{11.7}$$

Combining equations (11.6) and (11.7) with

$$v = r_w\omega_w, \quad T_{resist} = F_{resist}r_w, \quad T_w = F_w r_w \tag{11.8}$$

gives

$$\begin{aligned}\left(m + J_w/r_w^2\right)\dot{v} &= F_w - F_{dr} \\ &= F_w - F_{air} - F_{roll} - mg\sin(\alpha)\end{aligned} \tag{11.9}$$

As previously mentioned, the accelerometer measures the sum of the truck's acceleration and the part of the gravitation which lies in the trucks driving direction as

$$a_{sensor} = \dot{v} + g\sin(\alpha) \tag{11.10}$$

Combining equations (11.9) and (11.10) gives

$$\begin{aligned}\left(m + \frac{J_w}{r_w^2}\right)a_{sensor} &= F_w - F_{roll} - F_{air} + \frac{J_w}{r_w^2}g\sin(\alpha) \\ &= F_{resulting}\end{aligned} \tag{11.11}$$

It is desirable to make the estimation of the mass independent of the road slope estimation, since this is in itself an estimation. As can be seen equation (11.11) involves the road slope. However, a comparison of the values of the terms on the right side of the equality in (11.11) shows that the term involving the road slope is significantly smaller most of the time. Therefore, if only samples are used in the estimation when the driving force is big, the term involving the road slope can be neglected.

The adaption based on equation (11.11) is made with a Kalman filter algorithm. There are other algorithms for adaptive signal problems of this kind, like Least Mean Square (LMS) and Recursive Least Square (RLS), see [9], but the Kalman filter algorithm is more general and since the system is very simple in this case, the computations are simple. The model is now written as

$$\dot{\theta} \equiv \quad \tfrac{d}{dt}\left(m + \tfrac{J_w}{r_w^2}\right) \quad = w \tag{11.12}$$

$$y = \quad F_{resulting} \quad = a_{sensor}\theta + n \equiv \varphi^T\theta + n \tag{11.13}$$

where φ^T is defined as a_{sensor}, w is the process noise and n is the measurement noise.

To use the theory for the time variant Kalman filter, it is convenient to have the system on a time discrete form, and for simplicity, a Euler approximation given in equation 11.14 of the derivative is made

$$\dot{\theta} = \frac{\theta(t+1) - \theta(t)}{h} \tag{11.14}$$

Combining (11.12) and (11.14) gives

$$\begin{aligned} \theta(t+1) &= \theta(t) + hw(t) && (11.15) \\ y(t) &= \varphi(t)\theta(t) + n(t) && (11.16) \end{aligned}$$

For a system written on the form in equations (11.15)-(11.16), the algorithm for the adaptive Kalman filter is according to [9] given by

$$\begin{aligned} \hat{\theta}(t) &= \hat{\theta}(t-1) + K(t)[y(t) - \varphi^T(t)\hat{\theta}(t-1)] && (11.17) \\ K(t) &= \frac{P(t-1)\varphi(t)}{R(t) + \varphi^T(t)P(t-1)\varphi(t)} && (11.18) \\ P(t) &= P(t-1) - \frac{P(t-1)\varphi(t)\varphi^T(t)P(t-1)}{R(t) + \varphi^T(t)P(t-1)\varphi(t)} + Q(t) && (11.19) \end{aligned}$$

Q and R are the variances of w and n, and are the design parameters of the filter. P is the variance of the estimation. In this case all matrices are scalar, which makes the computations very simple. The filter has to be initialized with a value for the mass, $\hat{\theta}(0)$, and the variance of the initial value of the mass, $P(0)$. The values of Q and R is a balance between how fast the filter should be and how sensitive the filter is for measurement noise. More information about the filter can be found in [9].

To take into consideration that no estimation is to be made when the driving force is small, a threshold for this signal is inserted, meaning that K is put to zero during these samples and P is held constant. A similar threshold is made for cornering, as the accelerometer signal suffer from errors at these instances.

Since it is desirable to have a fast filter, that quickly adapt to a new weight after a reload, a high Q value is set. To achieve a stable output, all values are stored in a histogram and the peak of the histogram is set as output.

To validate the mass estimation, the truck ”Mastodont” is driven with two different loads. First it is driven without a trailer, making it very light. The weight is approximately 10.5 tons and the results of the mass estimation can be seen in figure 11.4. The weight adapts to a value of 11 tons, and considering that the resolution is set to one ton, this is considered to be correct. A second test can be seen in figure 11.5, where a trailer is attached to ”Mastodont” and the correct weight is just over 36 tons. The weight adapts to values of 36 and 37 tons which are considered to be correct values in this case as well. In both cases the weight adapts to a reasonable value after little over one minute.

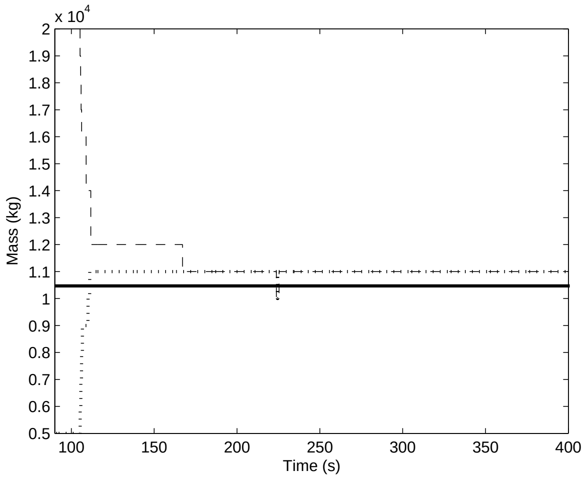

Figure 11.4. Mass estimations starting at 20 tons and 5 tons. The correct weight is given by the solid line.

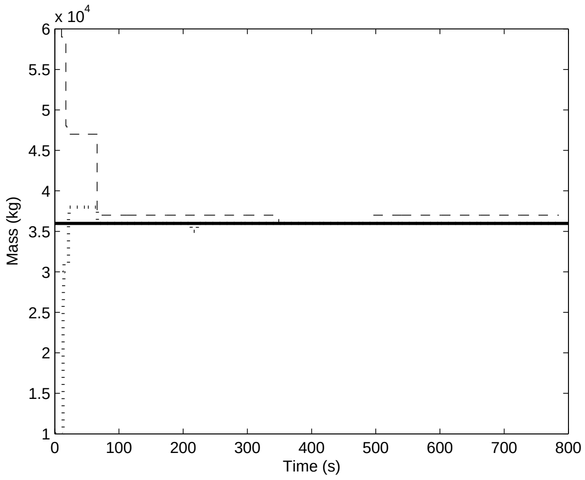

Figure 11.5. Mass estimation starting at 60 and 20 tons. Correct weight is given by the solid line.

11.9 Summary

An accelerometer is mounted in the truck and two different positions are evaluated. The best position is on the frame behind the cabin. Road slope and mass estimations are performed using the accelerometer signal. The road incline estimation is a good reflection of the actual road, but problems that arise from perpendicular acceleration during cornering have to be investigated in more detail. Due to limited time, no further investigation of compensation for disturbances from perpendicular acceleration is performed in this thesis. The mass estimation is fast and makes a good estimation of the actual vehicle weight.

Chapter 12

Simulation and Validation of the Observer

In this chapter the observer, including the accelerometer described in section 11.6, is validated and plots for the different outputs are shown. The recording used in the validation is made with the truck ”Mastodont” at the test course at Scania Technical Center. The accelerometer is placed behind the cabin on the frame of the truck.

12.1 Speed Signals and Torsion

In figure 12.1 a section of the observer signals for the speeds and the torsion together with the measured speed signals can be seen. The observer manages to achieve smooth speed signals in 100 Hz, that capture the main dynamics without any offset. The torsion shows a stepwise behavior which directly corresponds to the steps in the engine torque signal. Since no measurement of this signal is available, no good validation can be made. However, when zero torsion is passed through, a backlash in the cogs causes a rattle in the driveline which is visible in the measured transmission speed. Now, comparing the time when the estimated torsion passes zero with the measured transmission speed, it can in figure 12.2 be seen that a big oscillation is induced in the transmission speed at exactly the same time as the estimated torsion passes zero. This can be seen as a validation that the torsion passes zero at the right time.

In figure 12.3 a comparison between the result of low pass filtering the engine speed signal and using the observer to achieve smooth signals in 100 Hz is made. The picture shows the step the engine speed makes in the beginning of a gear shift, when it starts synchronization with the transmission speed of the new gear. The observer manages to give the same result as low-pass filtering without introducing any time delays, which is a great advantage.

During a gear shift, the goal is to get a signal that predicts the transmission speed without any oscillations. The transmission speed produced by the observer

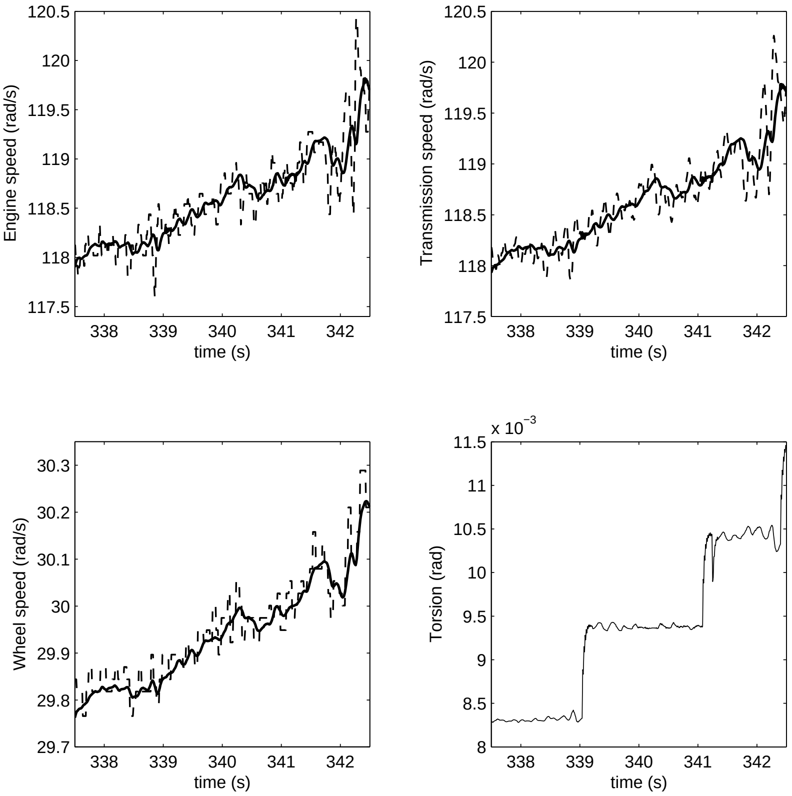

Figure 12.1. Measured signal is dashed and signal estimated in the observer is solid.

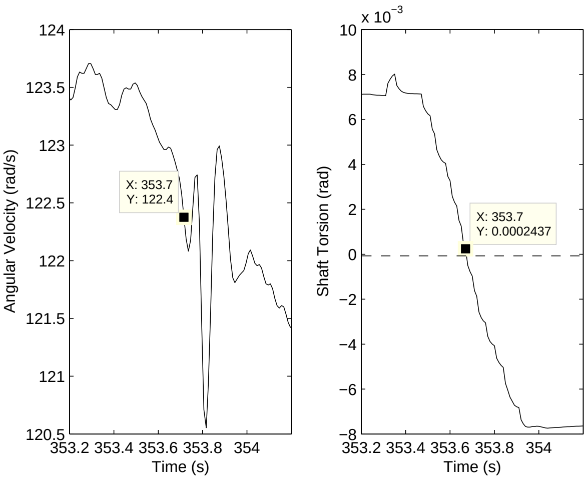

Figure 12.2. Left figure: Measured transmission speed. Right Figure: Estimated torsion.

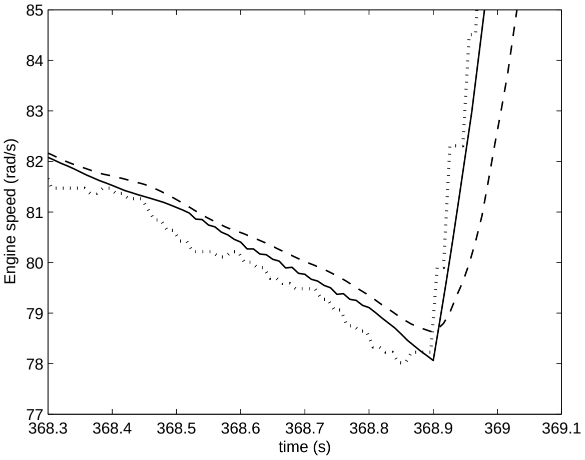

Figure 12.3. Measured engine speed (dotted), engine speed from observer (solid) and low pass filtered measured engine speed (dashed).

will capture some oscillations in the driveline. The oscillations arise from the torsion at the exact time of disengagement, which is hard to exactly predict. However, instead of using the observed transmission speed for this purpose, the wheel speed scaled with the transmission ratio of the final drive can be used.

In figure 12.4 the measured transmission speed and the scaled wheel speed from the observer can be seen during a gear shift. As can be seen the drive shaft works like a low-pass filter that remove the oscillations in the transmission speed. The dynamics of the shaft does not affect the offset between the signals.

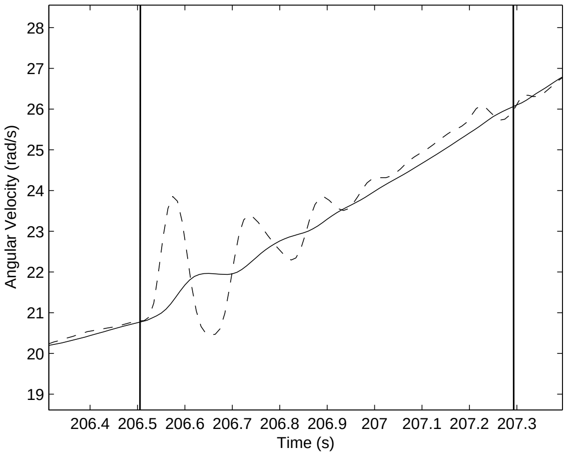

Figure 12.4. Measured transmission speed (dashed) and observed wheel speed scaled with the transmission ratio of the final drive. Between the vertical lines the gearbox is in neutral gear.

12.2 Road Slope

A segment of the road slope estimation made by the observer together with approximate markings taken from a map can be seen in figure 12.5. The result is satisfying and the road slope has a fast transient behavior without being sensitive toward noise. During the engagement of the disc brakes, the road slope still shows a good behavior.

12.3 Use of Disc Brakes during a Gear Shift

The results considered so far in this chapter are all satisfying. However, the case with a gear shift while the disc brakes are engaged, show less satisfying results for the speed signals. As can be seen in figure 12.6 the wheel speed show significant errors at each gear shift. This most likely has its origin in a false drive resistance estimated during braking, which in turn creates false estimates of the torsion at

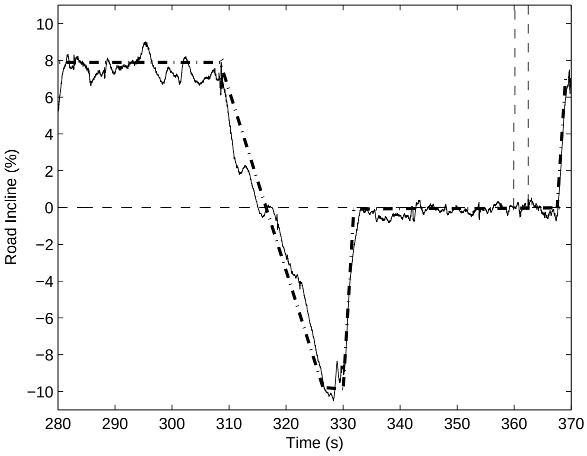

Figure 12.5. Road incline together with the supposed correct road incline (dash-dotted). Between vertical lines disc brakes are engaged.

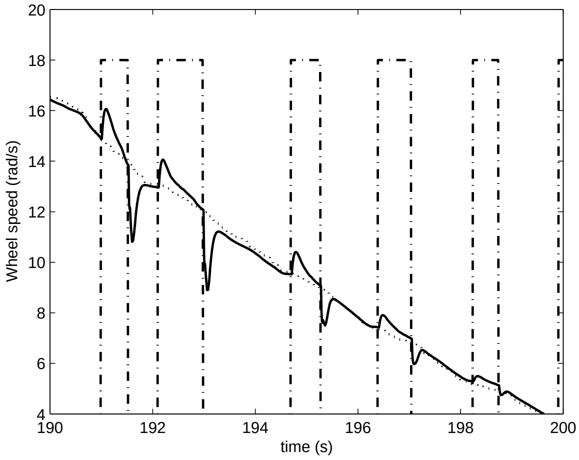

Figure 12.6. Observer wheel speed (solid) and measured wheel speed (dotted) during a period where the disc brakes are engaged. Dashed line represents when the gearbox is in neutral.

the engagement and disengagement of neutral gear. The false torsion creates bad estimations of the speed signals. More work on this topic is needed.

Chapter 13

Conclusions and Future Work

13.1 Conclusions

The aim of this thesis has been to investigate the benefits gained from implementing an observer of the driveline in the control system of a truck. The observer is a Kalman filter including a driveline model basically consisting of two masses connected by a torsional stiffness. The driveline model involves a number of different parameters and it has been shown that the observer is insensitive toward the main part of these. The stiffness and damping of the drive shaft however play an important role if the torsion and oscillations are to be captured accurately. Two on-line methods for estimating these parameters have been proposed. The method based on oscillations in the speed of the gearbox's outgoing shaft has shown promising results. It estimates both the stiffness and the damping in the driveline, but too low values of the damping are achieved. The stiffness is estimated in both the case of an engaged and a disengaged driveline, and for the engaged mode the values seem to correspond well to the mechanical values of the stiffnesses. This makes it questionable to use an estimation of the stiffness in the case of an engaged driveline for the applications in this thesis.

The driveline model is a rather big simplification of the real driveline, and some phenomenas like the backlash are not modeled. The clutch is assumed to be linear which is definitely not case in reality. These simplifications has the effect that not all oscillations are captured. The major dynamics are however captured accurately enough. Better input signals and further modeling of the clutch and backlash is needed to capture more oscillations.

A first goal has been to increase the resolution of the engine, transmission and wheel speed signals to 100 Hz and achieve smooth signals without introducing any time delays. This has proved to be possible with the use of the observer proposed in this thesis, and the results are for the most part satisfying. The objective to run the observer in 100 Hz is however dependent on the values of the parameters describing the stiffness and damping of the drive shaft. A stiffer driveline might demand smaller simulation steps than 0.01 seconds. It has also been shown that the observer is insensitive to the loss of one of the measurements. Some decrease in performance is however introduced during gear shifts if the engine speed is unavailable.

Replacing the Opticruise sensor by the tachograph has only a small influence on the estimated states even though the signal is highly low-pass filtered and time delayed. The small time delay on the estimated transmission speed using the tachograph signal is more troubling. Should this time delay not be a big concern, the Opticruise sensor would be redundant in the driveline observer and could be removed.

A second goal was to estimate the road slope with the use of the observer. This is based on a static model of the drive resistance and an unknown state for the road slope. This approach shows good ability to estimate the road slope, and together with the models for the rolling and air resistance it gives a driving resistance that has a fast transient behavior. The main disadvantage with this method is that it needs a model for the disc brakes to produce correct values of the road slope during braking. Better information about the brake drum pressure than currently available is needed to achieve a model for the brake torque. To work around this problem an accelerometer is a good alternative. It has been shown that with a one dimensional accelerometer, it is possible to get a good road slope estimation without knowledge of any brake force. Using this road slope should also make it possible to estimate the brake force, but results from this has not been presented in this thesis.

The accelerometer is also used to adaptively estimate the mass of the vehicle. The method described in the thesis has so far shown very good results and in a very short time the mass adapts to a correct value.

13.2 Future Work

The model proposed for the driveline captures the main dynamics, but if the goal is to also use the observer to create a controller for the oscillations in the driveline, more work is needed on the estimations of the stiffness and damping of the driveline. A real-time implementation of the estimation method is also required. The performance is to some degree also limited by the quality of the input signals. Extending the model with models of for example the engine and exhaust brake would therefore probably improve the quality of the observer. A clutch model may also improve the observer. Further, an automatic calibration of the accelerometer has to be developed to guarantee correct values from the sensor when for example removing or attaching a trailer, which makes the truck tilt. For trucks equipped with an air suspension system there exist information about the position of the suspensions. This information is believed to be useful in the road slope and mass estimation.

The model also has to be implemented and tested in a truck to check how the observer performs in a real time implementation at a processing rate of 100 Hz.

Further work is also needed to establish if different Kalman filters are needed for different trucks.

Notation

Variables and Signals	
ω_e	Angular velocity of the output shaft of the engine
ω_c	Angular velocity of the clutch
ω_t	Angular velocity of the output shaft of the gearbox
ω_p	Angular velocity of the input shaft of the final drive
ω_f	Angular velocity of the output shaft of the final drive
ω_h	Angular velocity of the input of the hub reduction
ω_w	Angular velocity of the wheel
α	Road incline
v	Velocity of the vehicle
a_{sensor}	Accelerometer signal
T_{comb}	Torque generated by the combustion engine
$T_{fr,e}$	Engine friction torque
$T_{parasitic}$	Torque on the output shaft of the engine from e.g. climate system
T_c	Torque on the shaft between the engine and the clutch
T_{exh}	Torque on the engine output shaft generated by increasing the pressure in the exhaust system
T_t	Torque on the shaft between the clutch and the input of the gearbox
T_p	Torque between the gearbox and the propeller shaft

Variables and Signals	
T_f	Torque between the propeller shaft and the final drive
T_d	Torque between the final drive and drive shaft
T_h	Torque between the drive shaft and the hub reduction
T_w	Torque between the hub reduction and the wheel
T_{dr}	Torque from the driving resistance
F_{roll}	Rolling resistance force
F_{air}	Force from the air drag
$F_{incline}$	Force arising from the road incline
F_{dr}	Drive resistance force. All forces acting on the body of the vehicle

Parameters	
J_e	Engine flywheel moment of inertia
J_t	Moment of inertia for the gearbox when it is engaged
$J_{t,in}$	Moment of inertia for the gearbox for the incoming axis when the gearbox is disengaged
$J_{t,out}$	Moment of inertia for the gearbox for the outgoing axis when the gearbox is disengaged
r_w	Rolling radius of the wheel
k_c	Spring stiffness in the clutch
c_c	Damping in the clutch
k_d	Spring stiffness in the drive shaft
c_d	Damping in the drive shaft
k_p	Spring stiffness in the propeller shaft
c_p	Damping in the propeller shaft
i_t	Transmission ratio of the gearbox
i_h	Transmission ratio of the hub reduction gear
i_f	Transmission ratio of the final drive
d_{sync}	Synchronization coefficient for engine and transmission speed after a gearshift
m	Mass of the vehicle
b	Friction coefficients
g	Gravitation on earth
$C_{r,iso}$	Constant in rolling resistance
C_a	Square constant in rolling resistance
C_b	Linear constant in rolling resistance
v_{iso}	Velocity during rolling resistance measurements according to ISO9948
ρ	Density of air
C_{drag}	Air drag coefficient
A_{front}	Projected front area of the vehicle

Term	
ABS	Anti-lock brake system
CAN	Computer area network. Protocol for network communication commonly used in the vehicle industry
NET	Department of transmission software.
OPC	Opticruise. Semi-automatic gear switch system.
Retarder	Hydraulic brake used in trucks as a complement to ordinary disc brakes.

Bibliography

[1] M. Petterson. *Driveline Modeling and Control*, Department of Electrical Engineering, Linköpings University, Linköping, Sweden 1997.

[2] J. Fredriksson. *Nonlinear Model-based Control of Automotive Powertrains*, Department of Signals and Systems, Chalmers University of Technology, Göteborg, Sweden 2002.

[3] M. Bruce. *Model Based Powertrain Control*, Department of Signals and Systems, Chalmers University of Technology, Göteborg, Sweden 2005.

[4] L. Nielsen, L. Eriksson. *Vehicular System*, Department of Electrical Engineering, Linköpings University, Linköping, Sweden 2005.

[5] E. Bråkenhielm. *Ett system för förarbedömning och förarträning i tunga fordon*, Master Thesis, Royal institute of technology, Stockholm, Sweden 2006.

[6] L. Råde, B. Westergren. *BETA, Mathematics Handbook for Science and Engineering*, Third Edition, Studentlitteratur Lund, Sweden.

[7] T. Glad, L. Ljung. *Reglerteori, flervariabla och olinjära metoder*, Second Edition, Studentlitteratur Lund, Sweden 2003.

[8] M. Berndtsson, E. Uhlin. *Skattning och aktiv dämpning av drivlinesvängningar i lastbil*, Master Thesis, Luleå Technical University, Luleå, Sweden 2003.

[9] F. Gustafsson, L. Ljung, M. Millnert. *Signalbehandling*, Second Edition, Studentlitteratur Lund, Sweden 2001.

[10] M. Satria, M.C. Best. *Comparison Between Kalman Filter and Robust Filter for Vehicle Dynamics State Estimation* SAE paper 2002-01-1185.

[11] T. Sandberg. *Modelling and Validation of Traveling Resistance for Heavy Trucks*, SAE paper 2001-01-0555.

[12] L. Nielsen, T. Sandberg. *A New Model For Rolling Resistance of Pneumatic Tires*, SAE paper 2002-01-1200.

[13] J. Y. Wong. *Theory of ground vehicles*, Second Edition, John Wiley & Sons, New York, United States of America, 1993.

[14] A. L. Dunn, G. J. Heydinger, G. Rizzoni, D. A. Guenther. *Empirical Models for Commercial Vehicle Brake Torque from Experimental Data*, SAE paper 2003-01-1325.

[15] P. Lingman, B. Schmidtbauer. *Road Slope and Vehicle Mass Estimation Using Kalman Filtering*, Vehicle System Dynamics Supplement 37, pp 12-23, 2002.

Appendix A

Truck Information

A.1 Mastodont

Mastodont (figure A.1) is a trailer-car, and is equipped with a 5.8 liter V8 engine. It has one front axle and two rear axles. The driving wheels are equipped with hub reduction gears making the driveline stiff. The gearbox has 12 normal gears and two crawl gears, summing up to 14 gears all together. The gearbox is overgeared, meaning that its' highest gear has a transmission ratio under one. The gearbox is

Figure A.1. Mastodont

equipped with the Opticruise system. Without any trailer attached its weight is approximately 12 tons.

A.2 Melvin

Melvin (figure A.2) is a normal truck equipped with a 4.7 liter 6 cylinder engine. It has one front axle and two rear axles. The gearbox has 12 normal gears and two crawl gears and is just like Mastodont overgeared. The gearbox is equipped with the Opticruise system.

SCANIA
SCANIA

Figure A.2. Melvin

Appendix B

Simulink Models

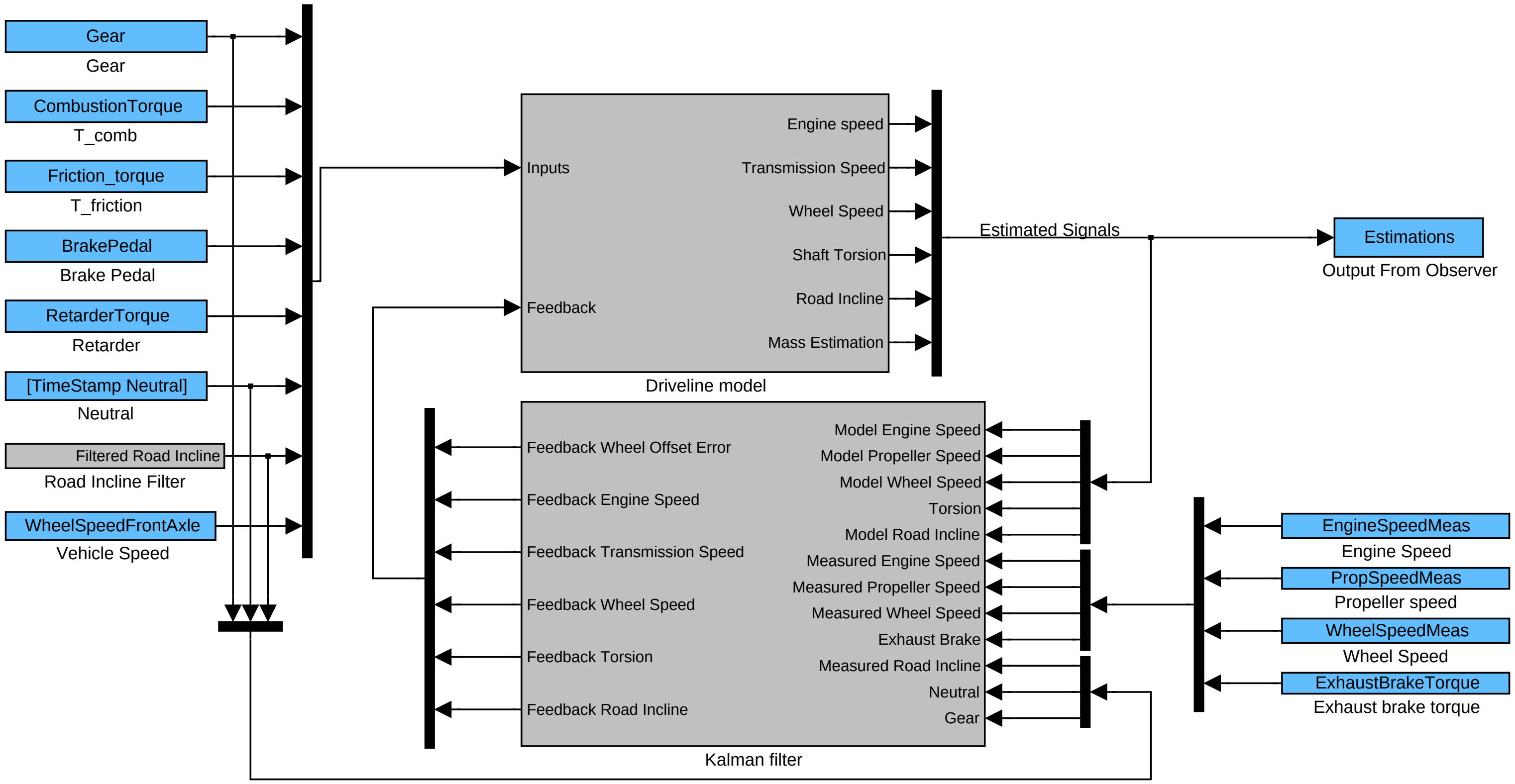
Gear
Gear
CombustionTorque
T_comb
Friction_torque
T_friction
BrakePedal
Brake Pedal
RetarderTorque
Retarder
[TimeStamp Neutral]
Neutral
Filtered Road Incline
Road Incline Filter
WheelSpeedFrontAxle
Vehicle Speed
Inputs
Feedback
Engine speed
Transmission Speed
Wheel Speed
Shaft Torsion
Road Incline
Mass Estimation
Driveline model
Estimated Signals
Estimations
Output From Observer
Feedback Wheel Offset Error
Feedback Engine Speed
Feedback Transmission Speed
Feedback Wheel Speed
Feedback Torsion
Feedback Road Incline
Model Engine Speed
Model Propeller Speed
Model Wheel Speed
Torsion
Model Road Incline
Measured Engine Speed
Measured Propeller Speed
Measured Wheel Speed
Exhaust Brake
Measured Road Incline
Neutral
Gear
Kalman filter
EngineSpeedMeas
Engine Speed
PropSpeedMeas
Propeller speed
WheelSpeedMeas
Wheel Speed
ExhaustBrakeTorque
Exhaust brake torque

Figure B.1. An overview of the Simulink implementation of the Observer

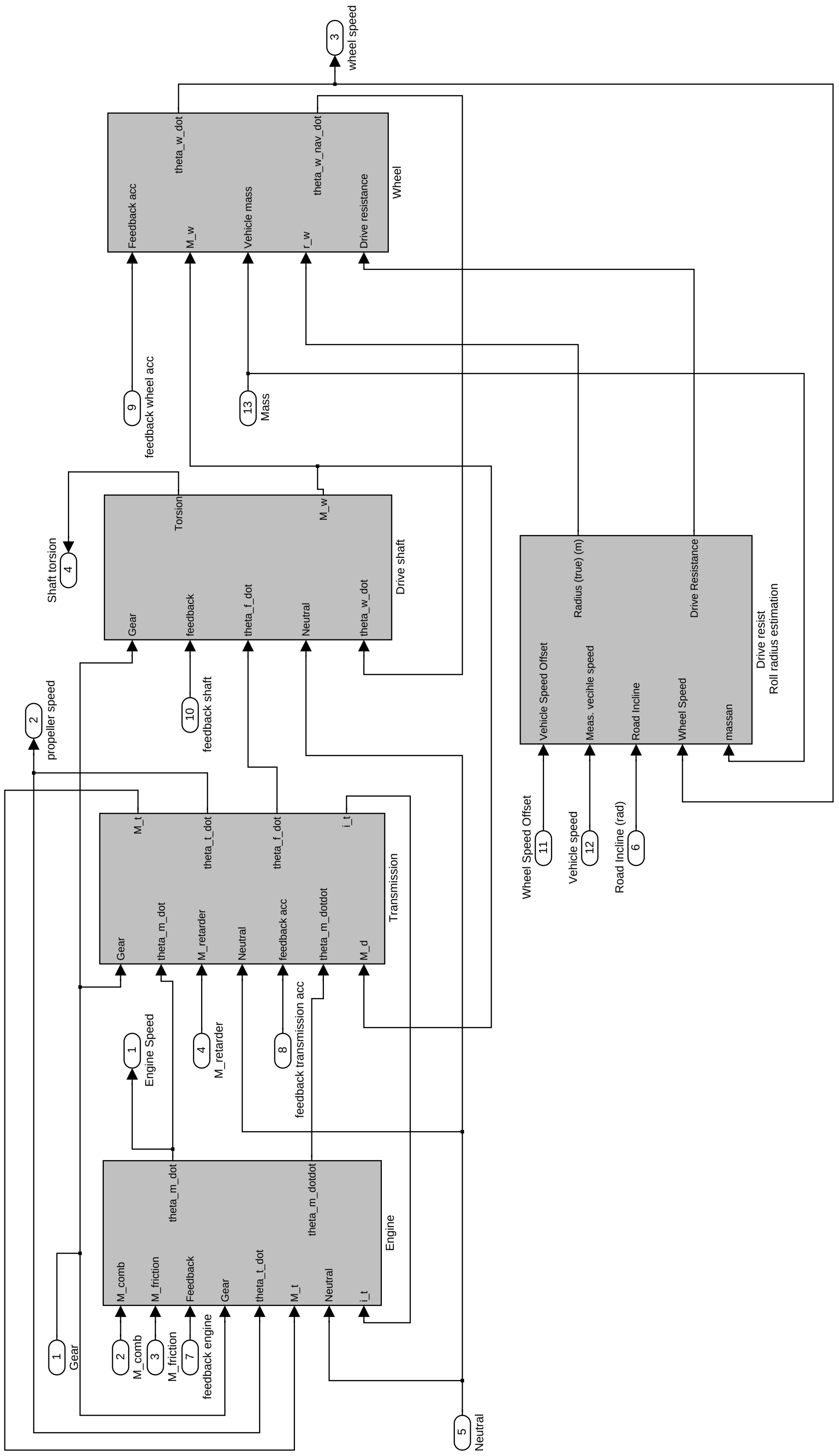
1
Gear
2
M_comb
3
M_friction
7
feedback engine
M_comb
M_friction
Feedback
Gear
theta_t_dot
M_t
Neutral
i_t
theta_m_dot
theta_m_dotdot
Engine
1
Engine Speed
4
M_retarder
8
feedback transmission acc
Gear
theta_m_dot
M_retarder
Neutral
feedback acc
theta_m_dotdot
M_d
M_t
theta_t_dot
theta_f_dot
i_t
Transmission
2
propeller speed
10
feedback shaft
Gear
feedback
theta_f_dot
Neutral
theta_w_dot
Torsion
M_w
Drive shaft
Shaft torsion
4
9
feedback wheel acc
13
Mass
Feedback acc
M_w
Vehicle mass
r_w
Drive resistance
theta_w_dot
theta_w_nav_dot
Wheel
3
wheel speed
5
Neutral
Wheel Speed Offset
11
Vehicle speed
12
Road Incline (rad)
6
Vehicle Speed Offset
Meas. vecihle speed
Road Incline
Wheel Speed
massan
Radius (true) (m)
Drive Resistance
Drive resist
Roll radius estimation

Figure B.2. An overview of the simulink implementation of the driveline model

Linköpings universitet

Upphovsrätt

Detta dokument hålls tillgängligt på Internet — eller dess framtida ersättare — under 25 år från publiceringsdatum under förutsättning att inga extraordinära omständigheter uppstår.

Tillgång till dokumentet innebär tillstånd för var och en att läsa, ladda ner, skriva ut enstaka kopior för enskilt bruk och att använda det oförändrat för ickekommersiell forskning och för undervisning. Överföring av upphovsrätten vid en senare tidpunkt kan inte upphäva detta tillstånd. All annan användning av dokumentet kräver upphovsmannens medgivande. För att garantera äktheten, säkerheten och tillgängligheten finns det lösningar av teknisk och administrativ art.

Upphovsmannens ideella rätt innefattar rätt att bli nämnd som upphovsman i den omfattning som god sed kräver vid användning av dokumentet på ovan beskrivna sätt samt skydd mot att dokumentet ändras eller presenteras i sådan form eller i sådant sammanhang som är kränkande för upphovsmannens litterära eller konstnärliga anseende eller egenart.

För ytterligare information om Linköping University Electronic Press se förlagets hemsida `http://www.ep.liu.se/`

Copyright

The publishers will keep this document online on the Internet — or its possible replacement — for a period of 25 years from the date of publication barring exceptional circumstances.

The online availability of the document implies a permanent permission for anyone to read, to download, to print out single copies for his/her own use and to use it unchanged for any non-commercial research and educational purpose. Subsequent transfers of copyright cannot revoke this permission. All other uses of the document are conditional on the consent of the copyright owner. The publisher has taken technical and administrative measures to assure authenticity, security and accessibility.

According to intellectual property law the author has the right to be mentioned when his/her work is accessed as described above and to be protected against infringement.

For additional information about the Linköping University Electronic Press and its procedures for publication and for assurance of document integrity, please refer to its www home page: `http://www.ep.liu.se/`

© Peter Juhlin-Dannfelt & Johan Stridkvist